



Localization of structural flaws in concrete sewer pipes by
physical interaction inspection with a robotic arm

E.J. (Edwin) van Boven

MSc Report

Committee:

H. Noshahri, MSc
Dr.ir. D. Dresscher
Prof.dr.ir. G.J.M. Krijnen
Dr.ir. L.L. Olde Scholtenhuis

May 2019

017RAM2019
Robotics and Mechatronics
EE-Math-CS
University of Twente
P.O. Box 217
7500 AE Enschede
The Netherlands

Contents

1	Introduction	1
1.1	Problem context	1
1.2	Problem statement	1
1.3	Research goal	2
1.4	Research questions	2
1.5	Outline	2
2	Analysis	3
2.1	Structural flaws in sewer pipes	3
2.2	Relation between material properties and structural flaws	8
2.3	Rebound principle of assessing concrete	13
2.4	Robotic assessment of concrete based on the rebound principle	22
2.5	Conclusion of analysis	25
3	Experimental Study	27
3.1	Design of experimental setup	27
3.2	Description of experiments	36
3.3	Validation of impact test	38
3.4	Influence of internal deflection of the robotic arm on measurements	42
3.5	Influence of spring settings on impact measurements	48
3.6	Influence of elastic modulus on impact measurement	51
3.7	Localization of flaws	55
3.8	Discussion of experimental study	59
4	Conclusion and recommendations	60
4.1	Conclusion	60
4.2	Discussion	61
4.3	Recommendations	61
A	Appendix Franka Emika Panda arm	63
	Bibliography	65

1 Introduction

This report studies the feasibility of locating structural flaws in concrete pipes due to interaction with a robotic arm. In this chapter the context of this research is given, the problem is stated and the goal of this research is given. Also the research question is stated and divided into sub-questions. At the end of this section, the outline of this report is given.

1.1 Problem context

The origin of this research lays within the TISCALI project (NWO, 2017), which is an abbreviation for ‘Technology Innovation for Sewer Condition Assessment - Long-distance Information-system’. This project focuses on automation and information distribution of sewer pipe inspection. An overview of the TISCALI project is given in figure 1.1.

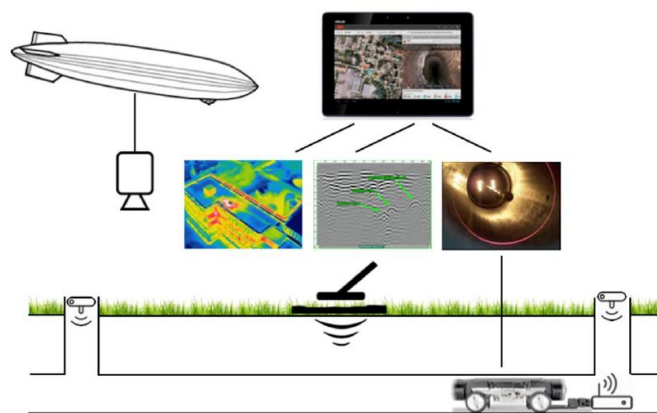


Figure 1.1: Overview of Tiscali Project (RAM, 2019)

In the overview the different aspects of the TISCALI project are shown. One can see the zeppelin, which represents inspection from higher altitude, in order to locate potential flaws in sewer pipe system. Another aspect shown, is a kind of sweeper on ground level. This represents inspection of the sewer pipes from ground level with ground-penetrating radar. Which is used to locate structural flaws more precisely, based on the information retrieved from high altitude inspection. In case a certain pipe has a potential flaw, in-pipe inspection is required in order to locate the exact position and the severity of the flaw. This is represented with the cart that is shown inside of the pipe. This research is part of the research done by the TISCALI project that is focused on automation of in-pipe sewer inspection.

1.2 Problem statement

In-pipe sewer inspections is currently done by visual inspection. Carts are enabled with CCTV which can move remotely through the sewer pipes. The videos have to be inspected manually. Research is already done on the automation of this visual aspect (Duran et al., 2002). However, to the knowledge of the author, no research is done on inspection of the sewer pipe by means of automated physical interaction with the sewer pipe. The physical interaction could be used in order to get information of the integrity of the sewer pipe. As CCTV can only see the inner surface of the sewer pipe, it is interesting to investigate if physical interaction with the sewer pipe can yield additional information on flaws that are not visible on the surface.

1.3 Research goal

The research described in this report covers the investigation of the feasibility of inspecting concrete with physical interaction. The physical inspection can be done in a variety of ways, but because time is limited, this research is only focused on physical interaction inspection with a robotic arm. The goal of this research is to determine if it is feasible to locate structural flaws in a sewer pipe by physically interacting with a robotic arm.

1.4 Research questions

As the goal is to study the feasibility of locating structural flaws by physically interacting with a robotic arm, the research question is formulated as following **'To what extent can interaction between a robotic arm and the surface of a concrete pipe be used to locate structural flaws of the pipe?'**

In order to give a structured answer on the research question, the question is divided into sub-questions. First it is important to determine which structural flaws occur in sewer pipes and which should be prioritized for location by physical interaction inspection. Which leads to the first subquestion: **Which structural flaws in sewer pipes can be located by physical interaction?**

Secondly the relation between physical properties of the concrete sewer pipes and these structural flaws has to be determined. **How do physical properties relate to the structural flaws of the pipe?**

Then a look will be given to the principle of the Schmidt hammer and the Leeb hammer, as these are two manual inspection tools that use physical interaction with the surface of concrete in order to inspect the sample. **What principle do the Schmidt hammer and Leeb hammer use to asses the concrete?**

At last it will be determined if the principle of these hammers can be used for inspection with a robotic arm by answering the last subquestion: **How can the rebound principle be used to locate structural flaws with a robotic arm?**

1.5 Outline

In this section an outline of the report is given. In the next chapter, chapter 2 an analysis will be conducted in order to give a theoretical answer to the research question. In the analysis a method will be proposed by answering the sub-questions individually. The proposed method to assess the concrete needs an experimental study. This experimental study on the proposed method is conducted in chapter 3. First the design of the experimental setup will be discussed. The performance of the method on locating flaws will also be discussed. In chapter 4 the conclusion of this research will be made and recommendations will be given for further research.

2 Analysis

In this chapter an analysis based on literature is conducted in order to answer the research question. The research question stated in the introduction is: 'To what extent can interaction between a robotic arm and the surface of a concrete pipe be used to locate structural flaws of the pipe?' This chapter is divided into the different sub-questions in order to answer them separately. First will be discussed which structural flaws in sewer pipes are to be located. Secondly there will be investigated which material properties of concrete sewer pipes relate to these structural flaws. Then a look will be given towards two inspection tools, the Schmidt hammer and the Leeb hammer, that use the rebound principle in order to assess a concrete sample. Accordingly will be investigated if this principle can also be used for a robotic arm in order to assess concrete. At the end of this chapter the separate answers will be combined into answering the research question theoretically.

2.1 Structural flaws in sewer pipes

In order to determine if a robotic arm can locate structural flaws in concrete sewer pipes by means of physical interaction, there should be determined which structural flaws occur in sewer pipes and which flaws are most relevant. The following sub-question needs to be answered in this section: **Which structural flaws in sewer pipes need to be located by physical interaction?**

First it will be investigated which flaws occur and how often they occur relative to the other flaws. Then additional information will be given on the flaws. For the flaws will also be discussed if the flaws are visible for CCTV during in-pipe inspection, as the physical interaction inspection could have additional value for flaws that are not visible during the current inspection method. At the end of this chapter will be discussed which flaws should have priority for physical interaction inspection.

2.1.1 Occurring structural flaws

To determine which structural flaws should be located with physical interaction, there should be investigated which flaws occur in sewer pipes and how often they occur. In this section there will be discussed which structural flaws occur in sewer pipes and how often they occur relative to the other flaws.

In figure 2.1 the distribution of defects of sewers in Germany is shown (Kaempfer and Berndt, 1999). While this graph is made in 1999, it gives a good indication of the occurring defects in sewer pipes.

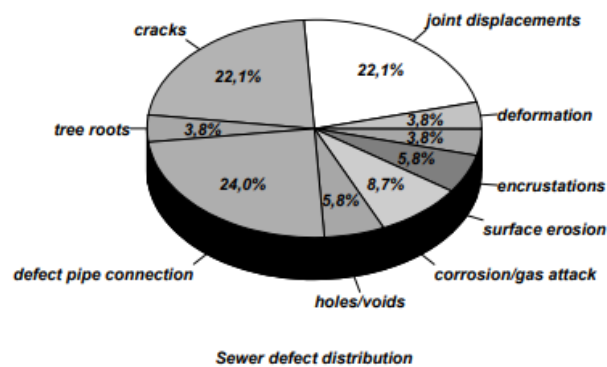


Figure 2.1: Example of concrete pipe (Kaempfer and Berndt, 1999)

The figure shows a clear distribution of the flaws. Joint displacements, defect pipe connections and cracks in pipes show to play the biggest part of flaws in the sewer pipe system. The flaws shown in the pie chart will be discussed in the following subsections. Most of the flaws are also mentioned by StateOfIndiana (2014). The report shows a variety of flaws that can occur on different parts of the pipe and what kind of flaws are acceptable and how to inspect the pipes visually. For visual inspection in The Netherlands the flaws are classified based on the standard NEN 3399:2015 nl. The standard describes how to classify the severity of the flaw, where the severity is rated a value between one and five. To gain knowledge on the classification of the standard and required countermeasures to certain flaws, it is advised to take a look at the standard.

2.1.2 Joint displacement and defect pipe connections

A large part of the flaws are joint displacements and defect pipe connections, as figure 2.1 shows. In figure 2.2¹ a joint displacement between two pipes is shown.



Figure 2.2: Joint displacement

The picture of a joint displacement shows that these flaws are visible on camera from the inside of the pipe. It is important to replace or repair joint displacements in case of severe joint displacements, as they can cause sink holes (Tacoma, 2019).

¹<https://www.goenviro.co.uk/drain-cleaning-services/cctv-drain-survey/>

No literature was found on the subject of defect pipe connections. Because no literature is found, the flaw is not considered to be relevant for this research. Therefore this flaw is left out of the scope of this research.

2.1.3 Cracks

Cracks are also a large part of the occurring flaws, as can be seen in figure 2.1. Figure 2.3 shows a sewer pipe with cracks.



Figure 2.3: Crack in a sewer pipe (Tacoma, 2019)

Cracks can cause leakage, which eventually can also cause voids behind the concrete (Karoui et al., 2018). According to Tacoma (2019), minor cracks do not affect the operational functionality of the pipe, but can increase in size and numbers. In case of increasing severity, repair or replacement is required (Tacoma, 2019).

2.1.4 Voids

While figure 2.1 showed that voids are only a small part of the occurring flaws, they can be very hazardous. People can fall down into a collapsing hole. An example is shown in figure 2.4², where a woman fell down in a sinkhole in the summer of 2018 in Limburg, The Netherlands.



Figure 2.4: Accident due to a void

Because of the danger caused by the voids it is important to detect voids. Voids do however exist behind the sewer pipe, so they are not visible on video during in-pipe inspection.

²<https://www.1limburg.nl/bizar-vrouw-zakt-door-de-stoep-en-raakt-gewond>

Voids often come into existence because of soil leaking into the sewer, of which an example is shown in figure 2.5³ (Carlson and Urquhart, 2006).

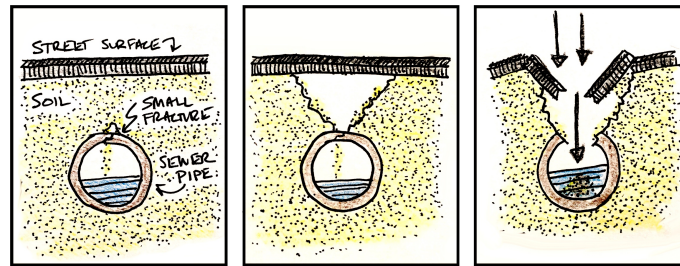


Figure 2.5: Possible cause of sinkholes

As the figure demonstrates, soil leaks slowly into the sewer through a small fracture. The water moves the leaked in soil away. The more soil leaked into the sewer pipe, the bigger the hole becomes, till at a certain point all the soil between the street and the sewer pipe is being washed away. As soon as a force is placed on the street surface, the tiles will not withstand the force and the structure will collapse.

2.1.5 Corrosion, surface erosion and encrustations

Corrosion, surface erosion and encrustations are flaws that occur on the inside of the pipe. As Kaempfer and Berndt (1999) mentions, the severity of corrosion depends on the surface pH value. Surface erosion and encrustations depend on the amount of water that flows through the pipe, but also what kind of stuff is dumped into the sewers (Kaempfer and Berndt, 1999). Figure 2.6⁴ shows the visible effect of corrosion on the sewer pipe. Figure 2.7⁵ illustrates the effect of encrustation in the pipe.



Figure 2.6: Corrosion on inner surface of pipe



Figure 2.7: Encrustation inside the sewer pipe

2.1.6 Tree roots

Tree roots also play a small role in the distribution of flaws in sewer pipes. Roots of trees occasionally grow into the pipe through cracks and joint displacements (Randrup et al., 2001). In figure 2.8⁶ an example of the flaw is given.

³<https://hoodline.com/2016/05/what-you-should-know-about-sinkholes>

⁴<http://www.maverickinspection.com/services/remote-video-inspection/rvi-video-imagery-gallery/drainage-systems/>

⁵<http://blog.envirosight.com/the-cost-of-sewer-pipe-corrosion>

⁶<https://www.wavin.com/en-en/News-Cases/News/Wavin-Insights-Sewer-blockages-caused-by-tree-roots>



Figure 2.8: Root growth inside sewer pipe

As the figure shows, tree roots are clearly visible on camera during in-pipe inspection.

2.1.7 Conclusion

In this section different types of flaws that can occur in sewer pipes are discussed in order to determine which flaws should be the focus of the localization method. Joint displacements, defect pipe connections, cracks, voids, corrosion, surface erosion, encrustations and tree roots are mentioned as potential flaws. Literature shows that joint displacements, defect pipe connections and cracks are the flaws that occur the most relative to the other flaws, as shown in figure 2.1. Most of the flaws are visible on camera. For voids this is however not the case. Also cracks are not visible, in the case when the cracks are not on the inner surface of the pipe. Because the voids and cracks are not always visible for visual inspection, this research will focus on the localization of cracks and voids. Because time is limited, localization of other flaws will not be investigated.

2.2 Relation between material properties and structural flaws

In the previous section the flaws that need to be located with physical interaction inspection is discussed. This section will discuss the relation between measurable physical properties and voids and cracks. Therefore this section will answer the following sub-question: **How do measurable physical properties of the concrete pipe relate to these structural flaws?**

In order to relate measurable physical properties to structural flaws, two measurable physical properties of concrete will be mentioned and explained: the elastic modulus and the compressive strength. At the end of this section a conclusion will be made of how the measurable physical parameters are influenced by the structural flaws.

2.2.1 Elastic modulus

The elastic modulus of a material is based on the relation between the stress and strain of the material. In order to determine the elastic modulus of a material, a force is applied on a cylinder of this material. This can be in the compression direction or in the tension direction. Figure 2.9⁷ will be used to explain how the elastic modulus of a material is determined.

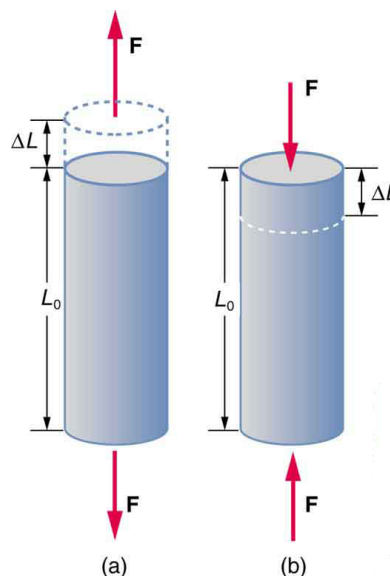


Figure 2.9: Deflection of a cylinder

The strain is determined by the difference in length, ΔL , divided by the original length L_0 . The stress is determined by the force, F divided by the area of the cylinder, A . When the stress on such a cylinder is plotted against the strain, it is called the stress strain curve. This stress-strain curve is shown in figure 2.10⁸.

⁷<https://opentextbc.ca/physicstestbook2/chapter/elasticity-stress-and-strain>

⁸<https://www.pavementinteractive.org/reference-desk/design/design-parameters/elastic-modulus/>

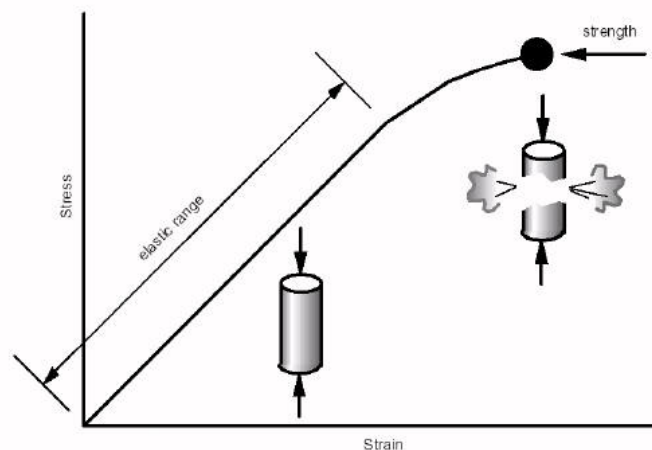


Figure 2.10: Stress strain relation

The elastic modulus is the relation between stress and strain in the elastic range of the stress strain curve. This relation is actually the slope of the curve, visible in figure 2.10. The elastic modulus of concrete is about 30 GPa⁹, but can be different for different kind of concretes, as it depends on how the concrete is made (Counto, 1964) (Hirsch, 1962). For comparison, the elastic modulus for rubber is between 0.001 GPa and 0.05 GPa¹⁰.

2.2.2 Compressive strength

The compressive stress under which the material breaks, is called the compressive strength. This is in the opposite direction with regard to the tensile strength, which is the tensile stress under which the material breaks. In figure 2.11¹¹ the stress-strain curve of brittle materials is shown, from which the tensile strength and the compressive strength can be interpreted.

Stress-Strain for Brittle Material (Tension & Compression)

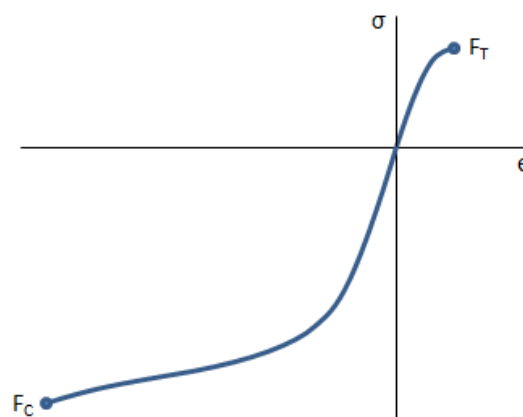


Figure 2.11: Stress strain relation for brittle materials

In the stress strain curve, the compressive strength is the stress on the lowest point of the curve, F_C . The tensile strength is the highest point on the curve, F_T . For metals the compressive strength and the tensile strength are similar (Tort et al., 2010). Concrete however, is stronger in compression than tension, which is also shown in figure 2.11. A rule of thumb is to assume that

⁹https://www.engineeringtoolbox.com/young-modulus-d_417.html

¹⁰<https://www.azom.com/properties.aspx?ArticleID=920>

¹¹<https://mechanicalc.com/reference/mechanical-properties-of-materials>

the compressive strength of concrete is ten times stronger than the tensile strength of concrete (Badarloo et al., 2018), where the compressive strength is on average 40 MPa ¹². In case of rubbers it is the other way around, the tensile strength is higher than the compressive strength (Al-Mosawi, 2015), the compressive strength of rubber is on average 7 MPa (Fediuc et al., 2013). Figure 2.10 is actually quite similar to figure 2.11, where the first figure did only show the tensile range.

The most reliable way to determine the compressive strength of concrete is to increase the applied force until it actually breaks. While this gives the most reliable value for the strength of the material, the tested material is afterwards destructed. This is the so called 'Destructive test'. For this test, a concrete cube or cylinder is crushed in a compressive strength test by pressing on the sample and increase the stress until it breaks. An example of the compressive strength test is shown in figure 2.12 ¹³.



Figure 2.12: Example of compressive strength test on concrete

The figure shows an example of the destructive test. As mentioned, the test destroys the sample, which makes it unsuited for testing concrete structures which are in use, like sewer pipes. There also exist quite some non-destructive methods which estimate the strength of the concrete structure. An example is the Schmidt hammer, which will be discussed in section 2.3.

2.2.3 Relation between measurable material properties and cracks in concrete

In order to determine if the measurable material properties are affected by cracks, research based on literature is conducted. Cracks appears to be related to the compressive strength of concrete (Vecchio and Collins, 1993), as cracks soften the material and consequently lower the compressive strength. Vonk (1992) states the following: 'Analysis of test results shows that the size effect in compressive softening is more complex than in tensile softening. Localization of cracking is present in compressive softening, but it has a more diffuse character than in tensile softening.' Micro cracks also reduce the elastic modulus, due to softening (Maruyama et al., 2014). Dyskin et al. (2003) studied the crack propagation in cement under uniaxial loading of initial 3D cracks, where the existence of initial cracks influenced the maximal loading capacity. The size and orientation of the crack have also influence on this maximal loading capacity. A reduction of the compressive strength due to cracks is to be expected in concrete, however

¹²https://www.engineeringtoolbox.com/young-modulus-d_417.html

¹³<https://civilblog.org/2013/05/10/compressive-strength-test-of-concrete-is516-1959/>

according to Vonk (1992) this relation has a diffuse character, so it is not certain that this flaw will be measured. As time is limited, this research will not focus on the microscopic influence of cracks on the material behavior. Additional research is however required on how cracks influence the strength of the material, especially how they influence the compressive strength and elastic modulus of the material.

2.2.4 Relation between measurable material properties and voids in concrete

Research is also conducted on the relation between the measurable material properties and voids in concrete. Comparable to cracks, voids also reduce the compressive strength of the concrete (Ezeokonwo, 2000). Ezeokonwo (2000) tested different strengths of concrete with voids with different sizes and different orientations. Figure 2.13 shows the relation between the size and orientation of a void on concrete.

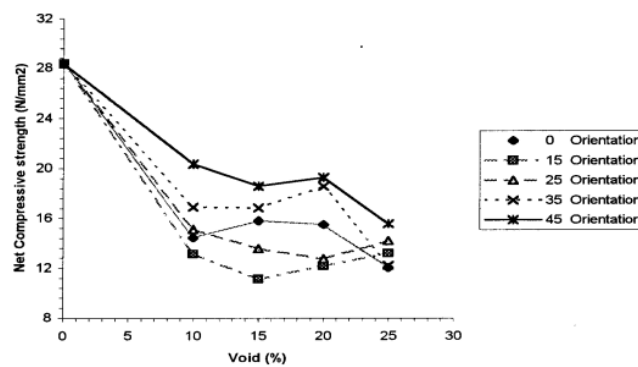


Figure 2.13: Influence of size and orientation of void on compressive strength (Ezeokonwo, 2000)

The figure clearly shows a decrease of compressive strength of the concrete due to the presence of a void. As well as the size as the orientation of the void influence the compressive strength. On the contrary, small air voids in concrete do actually increase strength of the concrete (Warren, 1953).

To gain insight on the influence of a void in a concrete tile on the strength of the tile, a finite element study has been conducted. A simulation has been done in order to calculate the deflection caused by a load on the tile. This is also done for a tile with a void. Both deflections can be compared in order investigate the influence of a void. These simulations were conducted in COMSOL Multiphysics. The used variables are shown in table 2.1 and the result is shown in figure 2.14.

Table 2.1: Displacement estimation with Elastic modulus

Variable	Value	Unit
Force	50	N
Elastic modulus	30	GPa
Diameter of contact point	3	mm
Thickness of the tile	40	mm
Thickness of the hole	20	mm

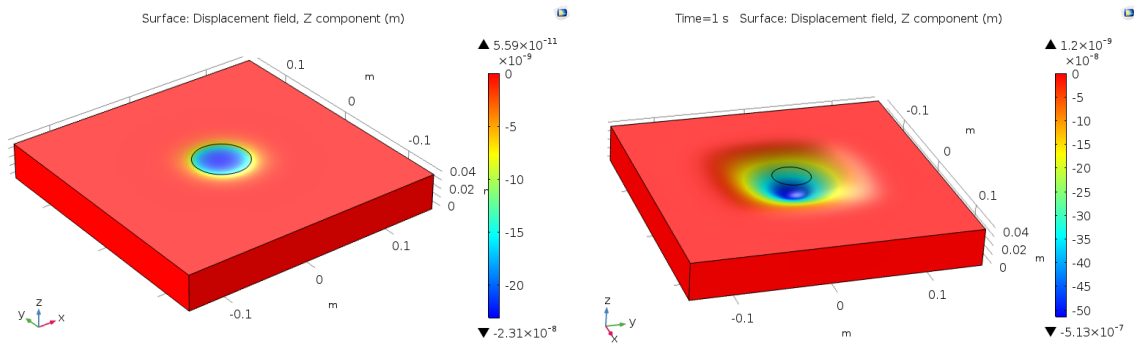


Figure 2.14: Modelled deflection of tile in COMSOL **Figure 2.15:** Modelled deflection of damaged tile

The largest displacement is in the middle of the undamaged tile, at the point of pressing, and is $0.0231 \mu\text{m}$. In figure 2.15 the simulation is shown in the case of a damaged tile, where the largest displacement is $0.962 \mu\text{m}$. The displacement on the tile with a void is about forty times larger than the tile without any damage. This simulation indicates a decrease in strength for a big void, however, no literature could be found on that subject. There needs to be noticed that in both cases the displacement is very small.

2.2.5 Conclusion

In this section the relation between measurable properties of concrete and flaws has been discussed. First information on the compressive strength and the elastic modulus is given. Then cracks are related to the measurable physical properties compressive strength and elastic modulus, where cracks decrease the compressive strength and micro cracks decrease the elastic modulus. Voids do also decrease the compressive strength of concrete. Very small air voids however, increase the elastic modulus of the concrete. A big void behind the surface is also expected to decrease the strength, but no literature could be found on that subject.

2.3 Rebound principle of assessing concrete

In the previous section the relations between the elastic modulus and the compressive strength and potential flaws are shown. In this section will be discussed how the rebound hammer is able to determine the compressive strength of concrete and the hammer will be compared with the Leeb hammer, which uses an impact to determine the hardness of the material. The working principle of the Leeb hammer and the Schimdt hammer will be investigated. In this section an answer will be given on the following question: **What principle do the Schmidt hammer and Leeb hammer use to asses the concrete?**

Firstly, an explanation will be given on how the rebound hammer works and how to operate the hammer. Next its principle will be explained. Secondly, the working principle of the Leeb hammer will be explained. The leeb hammer and the rebound hammer will be compared and it will be discussed what the hammers actually measure. Accordingly an answer will be given on the sub-question.

2.3.1 Rebound hammer

The rebound hammer is used in the civil engineering to determine the compressive strength on-site. In this section is explained how the hammer works and its required conditions are mentioned. Then the principle of the hammer will explored more deeply in order to determine what the hammer actually measures.

In order to explain how the rebound hammer works, different states of the hammer are shown in figure 2.16.

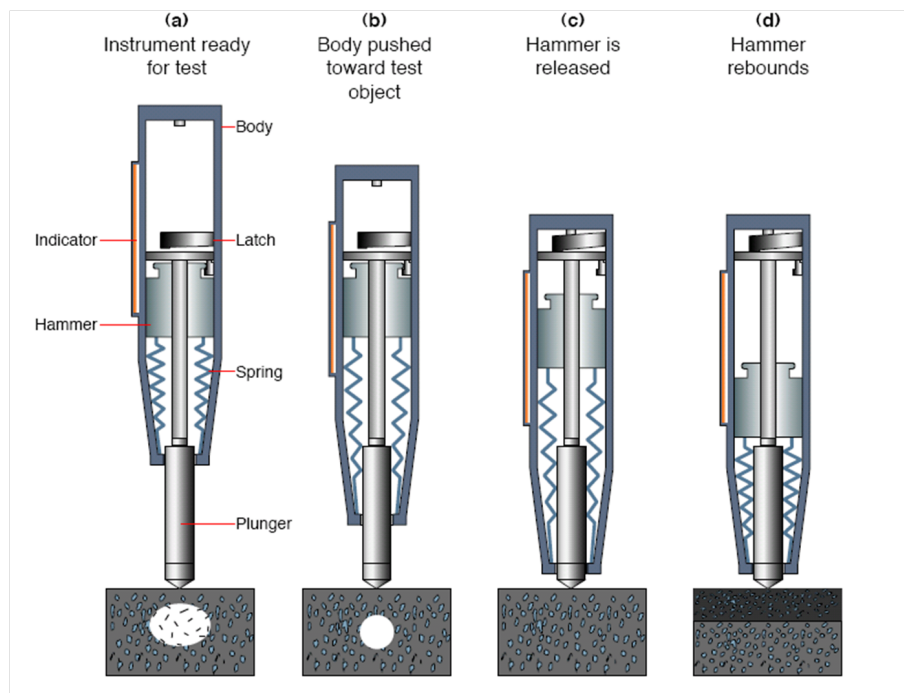


Figure 2.16: Different stages rebound hammer (Kvgd and Yelisetty, 2014)

In the first state, a), the rebound hammer is in rest. A force applied by the user is used to tension the spring, as can be seen in the second state, b). When the spring is under maximal tension, the hammer can be released. When released, c), the spring will act a force on the hammer, so the hammer accelerates. As soon as the hammer hits the plunger, the plunger will hit the surface. The plunger will rebound on the surface and will therefore rebound the hammer ,d). The distance the hammer rebounds is measured and shown on the indicator. Indication of zero

means the hammer did not bounce back and a value of one hundred means the hammer did bounce the whole distance back. Based on these distances the rebound value is determined and shown on the indicator. This rebound value is a relative indication of the strength of the material, where the rebound value can be used for comparison of the strength between two samples under similar conditions. In practice it is desired to relate the rebound value to the compressive strength of the sample. In order to do so, the hammer needs to be calibrated on a calibration anvil. After calibration the rebound value can be used to determine the compressive strength using a conversion. Figure 2.17 shows a conversion figure to estimate the compressive strength of the sample based on the measured rebound value, for the N/NR Schmidt hammer (EngineersDaily, 2019). Figure 2.18 shows the conversion graph for a L/LR Schmidt hammer.

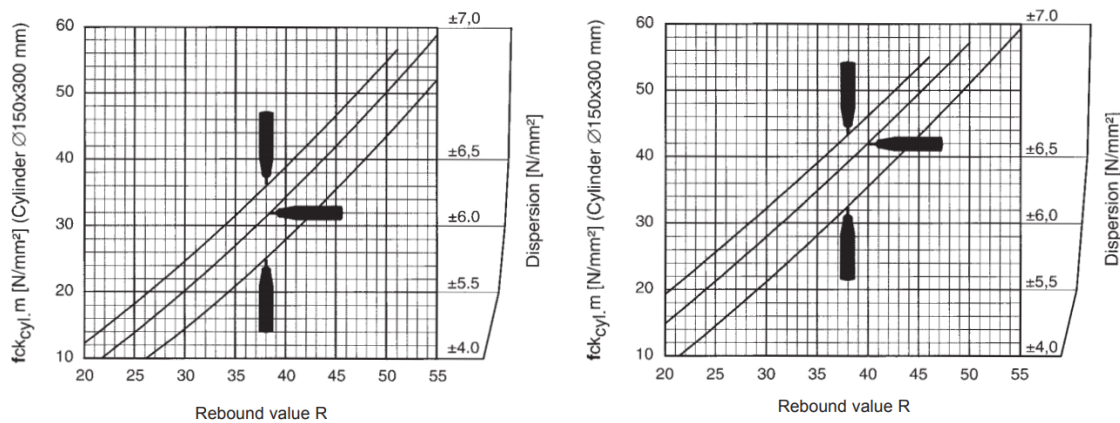


Figure 2.17: Conversion graph for N/NR Schmidt hammer (EngineersDaily, 2019) **Figure 2.18:** Conversion graph for L/LR Schmidt hammer (EngineersDaily, 2019)

The conversion curve shown in the figure, only holds for tests on a concrete cube, with sides of 150mm. The sample should have a smooth, dry surface, without any flaws in the cube. The concrete also should have an age between 14 and 56 days. The maximal diameter of the aggregate has to be 32 mm. In case the conditions differ from the required conditions for the conversion table, a factor is required in order to relate to the compressive strength. In the manual and literature certain formula are described which can be used to apply a factor to the measured rebound value to determine the rebound value of the material. The required conditions are quite a limitation on the technique, as unknown deviations give an error in the estimation of the compressive strength. Another limitation is the accuracy of the rebound method, as the method is very inaccurate. To get a good indication of the strength of the material and reduce the effect of the inaccuracies, it is advised to do a minimum of ten measurements and take the average value (ReboundGuide, 1993). The graph in figure 2.17 shows three lines, each with a position of the hammer drawn. This illustrates the effect of the orientation on the conversion between the rebound value and the compressive strength. This conversion is required as the gravity influences the measured rebound value. Figure 2.17 also mentions that the conversion table is to be used for the N/NR hammer. This N-type hammer is a hammer that uses an impact energy of 2.2J and is supposed to be used on concrete with a thickness between 50 mm and 100 mm. Another rebound hammer is the L/LR hammer, which is an hammer that uses an impact energy of 0.72 J (ReboundGuide, 1993). What can be seen in the conversion graphs in figure 2.17 and figure 2.18 is that the LR hammer has a higher rebound value for samples with the same strength. This gives an indication, that a higher impact energy results in measuring a higher rebound value.

In order to get a better idea of what the rebound hammer actually measures, further analysis on the rebound hammer and the rebound value is conducted. Equation 2.1 shows how to de-

termine the rebound value, where the rebound value depends on the initial position and the position to which the hammer bounces back.

$$R = \frac{x_r}{x_0} (\cdot 100) \quad (2.1)$$

Where R is the rebound value. The rebound value is multiplied by 100 so it actually shows a percentage, in future equations the value without the multiplication of 100 is used. x_r is the measured rebound distance and x_0 is the start position of the hammer. The impact energy originates from the initial stored energy in the system, which is the spring energy. The formula for this energy is shown in equation 2.2.

$$E_{k,0} = \frac{1}{2} C x_0^2 \quad (2.2)$$

Where $E_{k,0}$ is the initial energy, which is the spring energy. C is the spring constant of the rebound hammer. When assuming the influence of friction and gravity can be neglected, where the influence of gravity can be neglected in the case of applying a horizontal impact, all this energy converts into kinetic energy. On the moment of impact this kinetic energy will cause the material to deform partially elastic and partially plastic. When the energy lost to heat and the creation of sound is neglected, all the energy is converted into either strain energy or energy stored into plastic deformation.

The strain energy will convert into kinetic energy of the hammer at the end of the impact, when it will move the hammer back up. The energy stored into plastic deformation will be lost. The maximal strain energy can be estimated by equation 2.3.

$$E_{\text{strain}} = \frac{1}{2} C x_r^2 = \frac{1}{2} C \cdot x_0^2 \frac{x_r^2}{x_0^2} = E_0 \cdot R^2 \quad (2.3)$$

Where R is the rebound value, shown in equation 2.1. E_0 is the initial energy, shown in equation 2.2. The energy lost due to the plastic deformation can therefore be approximated by equation 2.4, because it is assumed that the energy lost to plastic deformation is the initial energy minus the strain energy.

$$E_{\text{plastic}} = E_0 - E_{\text{strain}} = E_0(1 - R^2) \quad (2.4)$$

These equations mainly show that the rebound value measures the plastic deformation caused by the impact. As Szilágyi et al. (2015) states "The value of the coefficient of restitution depends on energy losses due to dissipation by reflections and attenuation of mechanical waves inside the steel plunger and energy losses due to dissipation by concrete crushing under the tip of the plunger. This latter loss of energy makes the rebound hammer suitable for strength estimation of concrete. The energy dissipated in the concrete during local crushing initiated by the impact depends both on concrete compressive strength and Young's modulus; therefore, depends on the stress-strain ($\sigma - \epsilon$) response of the concrete tested."

A relatively new rebound hammer, the Silver Schmidt Hammer has almost an identical working principle as the regular Schmidt Hammer. It does however compare the impact velocity with the rebound velocity instead of comparing the starting position with the rebound position. The results of the Silver Schmidt Hammer are not influenced by the direction of the measurements

related to the gravity. The output velocity divided by the input velocity is called the true rebound coefficient, as shown in the following equation.

$$Q = \frac{v_{\text{out}}}{v_{\text{in}}} \quad (2.5)$$

Where Q is the true rebound coefficient, v_{out} is the velocity after the impact and v_{in} is the velocity before the impact. According to the research of Winkler and Matthews (2014) the Silver Schmidt Hammer realizes comparable results. This makes a lot of sense when looking at the initial energy and rebound energy again. Instead of looking at the initial spring energy, a look will be given to the initial kinetic energy.

$$E_{\text{kin},0} = \frac{1}{2} m v_{\text{in}}^2 \quad (2.6)$$

The energy after the impact can be based on the kinetic energy based on the velocity after the impact.

$$E_{\text{rebound}} = \frac{1}{2} m v_{\text{out}}^2 \quad (2.7)$$

Rewriting this equation will give the following equation.

$$E_{\text{rebound}} = \frac{1}{2} m v_{\text{in}}^2 \cdot \frac{v_{\text{out}}^2}{v_{\text{in}}^2} = E_0 \cdot \frac{v_{\text{out}}^2}{v_{\text{in}}^2} \quad (2.8)$$

This shows the same structure as 2.3, where the first part is equal to 2.6 and the second part to the rebound value. This gives the following equation for the rebound value.

$$Q = \frac{v_{\text{out}}}{v_{\text{in}}} \approx R = \frac{x_{\text{out}}}{x_{\text{in}}} \quad (2.9)$$

Contrary to the rebound value, Q is not influenced by the gravity so conversion based on the direction of the gravity is not required. As this equation shows that the different type of measuring should give similar results. It is important to remember the made assumptions; The effects of friction and viscous energy dissipation are disregarded. In reality these effects will influence the measurements. The influence of these effects are shown in figure 2.19. This figure shows the model of the energy balance during an impact (Patel et al., 2014). This study uses a model with a low-velocity impact, where the velocity of impact is considered 1 ms^{-1} to 3 ms^{-1} , using ABAQUS Explicit. In figure 2.19 the impactor mass is 2.6 kg, the velocity 3 ms^{-1} and the longitudinal compressive strength of the sample is considered 350 MPa (Aslan et al., 2003), which is higher than the compressive strength of concrete.

As the figure shows, the kinetic energy, in this case 12 J, is mainly converted into strain energy, which then converts back into kinetic energy. Energy is also lost to frictional dissipation, viscous dissipation and artificial strain energy. The final artificial strain energy can be considered as the plastic deformation. The figure shows that while the frictional dissipation and the viscous dissipation is small, it influences the energy lost during an impact.

2.3.2 Leeb hammer

In this section the working principle of the leeb hammer will be analyzed. The Leeb hammer uses an impact energy of 11 mJ and is considered to measure the hardness of a sample (YILMAZ and GÖKTAN, 2018). Figure 2.20 shows the working principle of this leeb hammer (Kovler et al., 2018a).

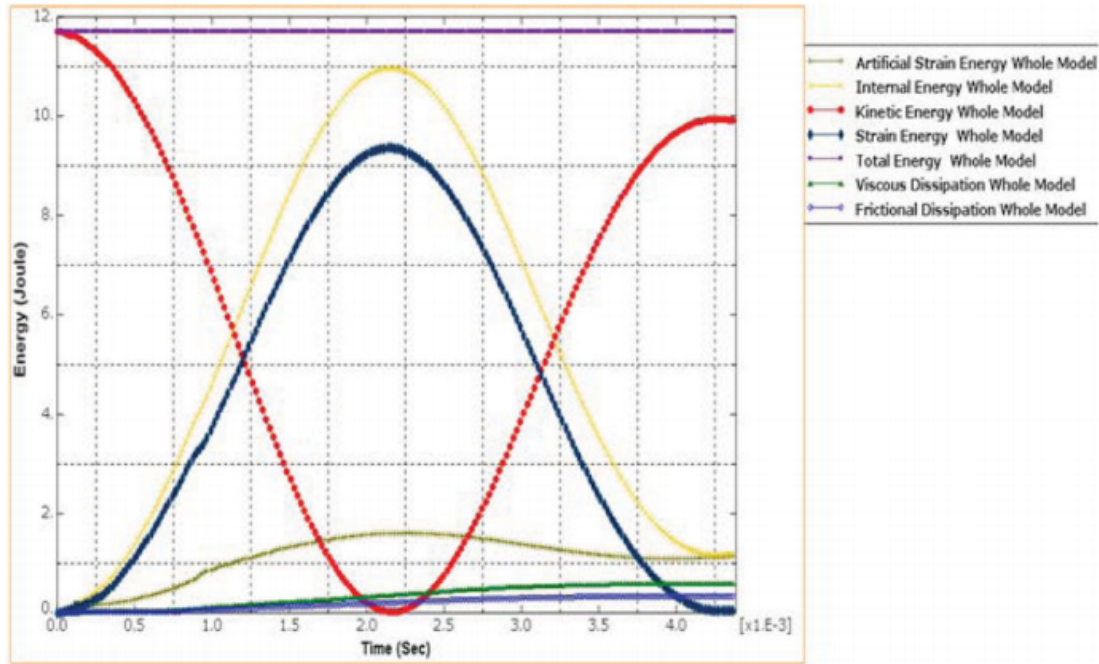


Figure 2.19: Impact model of Patel et al. (2014)

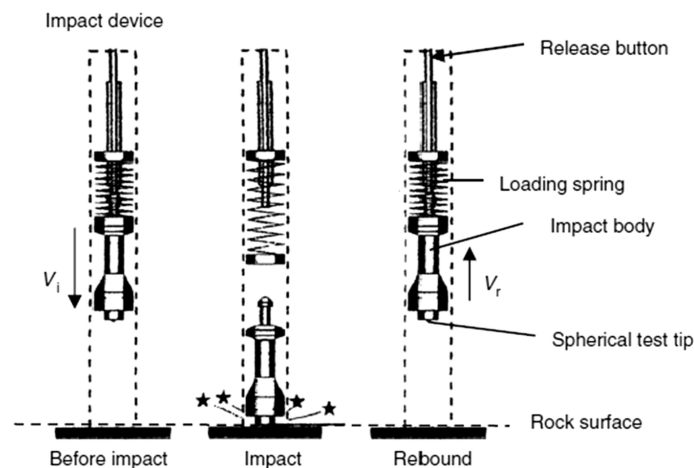


Figure 2.20: Description of working principle of Leeb hammer (Kovler et al., 2018a)

The loaded spring will cause the impact body to move with a certain velocity. The impact will cause the impact body to rebound. The relation between the rebound velocity and the input velocity is used to determine the hardness of the body tested. The Leeb hardness is determined on these velocities according to the following equation.

$$HL = \frac{v_{out}}{v_{in}} \cdot 1000 \quad (2.10)$$

Where v_{out} is the rebound velocity, v_{in} the impact velocity and HL the Leeb hardness. The Leeb hardness can be related to other hardness tests of materials like the Rockwell hardness, but should be done with care (Kompatscher, 2004). Kompatscher (2004) mentions the dependency on the elastic modulus of the testing method, which is demonstrated in figure 2.21.

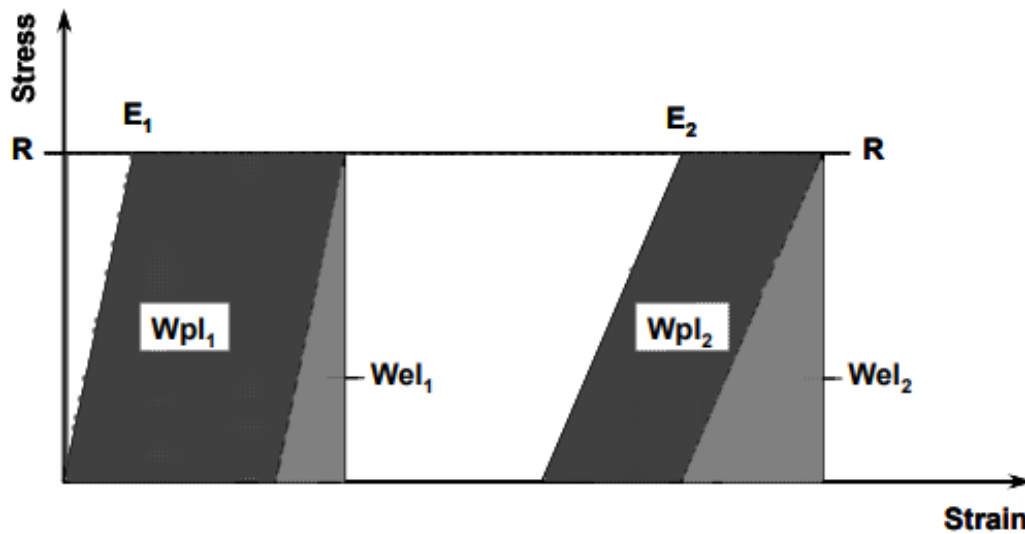


Figure 2.21: Influence of elastic modulus on rebound hammer (Kompatscher, 2004)

This figure is a simplified representation of the stress-strain curves of two materials with the same compressive strength, but different elastic moduli. In the figure R stands for the Yield strength, which is equal for both materials shown in the graph. E_1 and E_2 stand for the elastic modulus of the two materials. The relation between Wel_1 and Wpl_1 yields a significantly higher value than the relation between Wel_2 and Wpl_2 while the yield strength is equal. This illustrates that a material with a lower elastic modulus will yield a higher rebound value, while the compressive strengths are equal.

2.3.3 Comparison of Rebound hammer and Leeb hammer

In this section the rebound hammer and the leeb hammer will be compared. Both hammers use the rebound principle. However, the leeb hammer uses a much lower impact energy. On top of that, contrary to the regular Schmidt hammer, the rebound value of the leeb hammer and the Silver Schmidt hammer are not influenced by the direction of the test with regard to the direction of gravity. The figures 2.22 and 2.23 show the relation between their rebound number and the compressive strength (Kovler et al., 2018b).

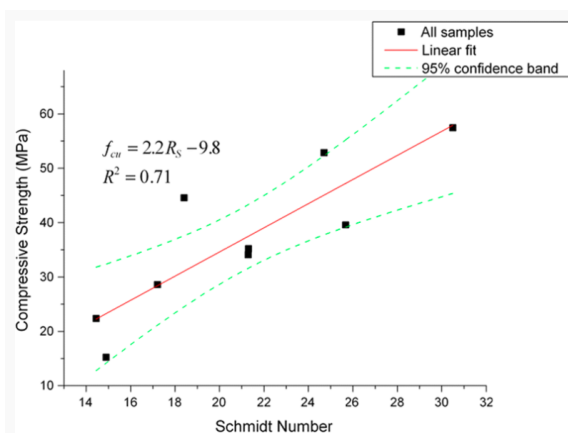


Figure 2.22: Relation between rebound value and compressive strength.

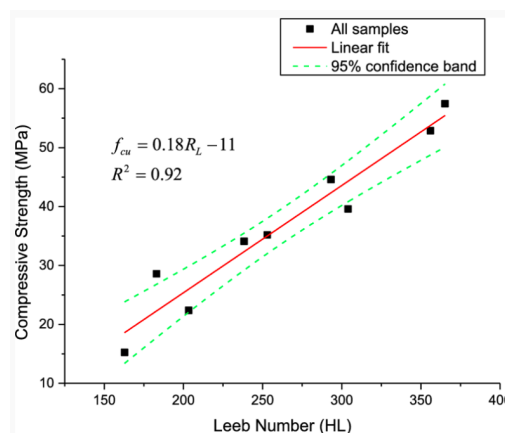


Figure 2.23: Relation between Leeb hardness value and compressive strength

The figures show that the Leeb hammer is in the study of (Kovler et al., 2018b), quite more accurate in determining the compressive strength of a material than the regular rebound hammer, as the confidence band is much smaller. On the contrary, Szilágyi et al. (2015) claims that the Leeb hammer rebound value is actually more related to the elastic modulus of the material than the compressive strength, due to the low impact energy. Szilágyi et al. (2015) supports the latter claim by figure 2.24 (Szilágyi et al., 2015).

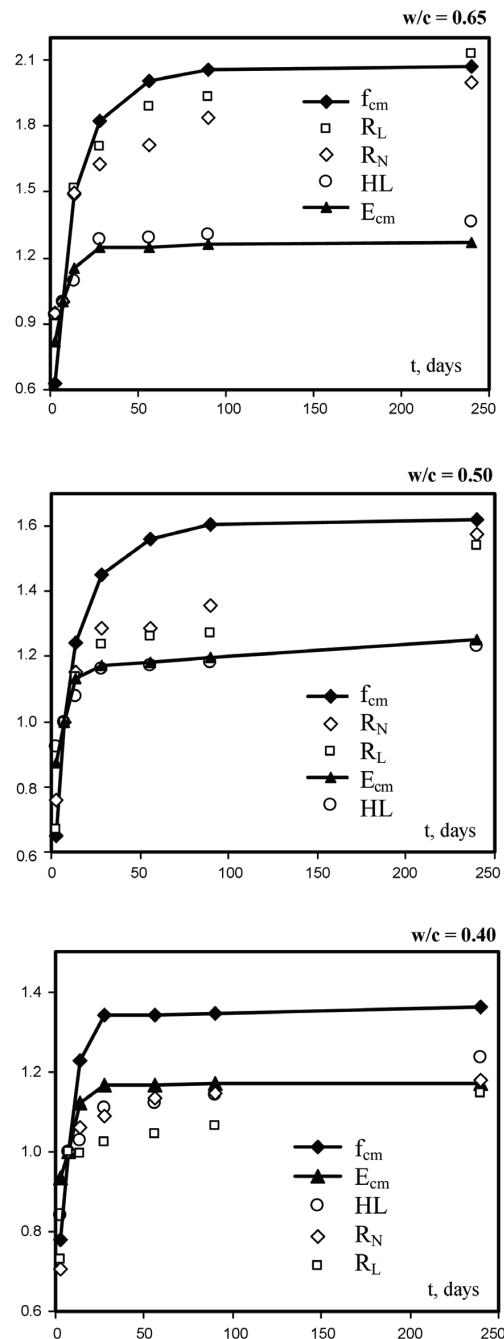


Figure 2.24: Relative change of modulus, strength and rebound values over aging of concrete.

Where f_{cm} is the compressive strength of the concrete sample over time and E_{cm} is the elastic modulus of the concrete sample over time. HL represents the measured leeb value on the concrete, R_N and R_L represents the rebound values of the two different Schmidt hammers.

In the study, three different mixtures of concrete are tested, where the w/c ratio is the ratio between the water and the cement. The mixture of 0.4 w/c has a significantly higher compressive strength and elastic modulus than the mixtures with a higher w/c ratio. What can be seen in the figure is that the strength over time increases as the concrete dries. The figures shows that the Leeb hammer values correlate with the elastic modulus. The rebound hammer correlates with the compressive strength for mixtures with a higher w/c, but also correlates with the elastic modulus for the concrete with a 0.4 w/c ratio. Szilágyi et al. (2015) concluded the following: "Results demonstrated that the rebound hammers could provide a hardness value that can be correlated to the compressive strength of concrete only if the compressive strength is relatively low. It was confirmed for high strength concretes that the Schmidt rebound hammers provide a hardness value that can be correlated to the Young's modulus of concrete rather than the compressive strength."

However, the study uses the development of the elastic modulus and the compressive strength of concrete over time. The study therefore neglects other effects that happen over time with the concrete that can influence the measured rebound values with the different hammers.

Kovler et al. (2018a) also compared the values given by the Schmidt hammer and the Leeb hammer. This comparison is shown in figure 2.25.

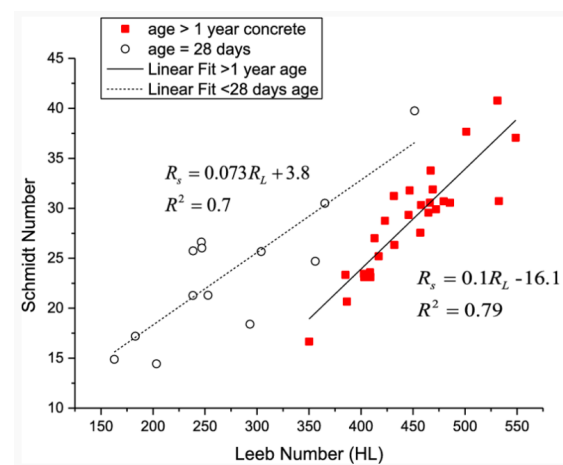


Figure 2.25: Comparison between Schmidt hammer and Leeb hammer (Kovler et al., 2018b)

In the figure values on relatively young concrete are shown and values on old concrete are shown. Kovler et al. (2018a) expects that the difference in relation between the hammers can be explained due to the fact that the Leeb hammer measures on the surface, where this surface is greatly influenced by aging due to carbonation. The Schmidt hammer is less influenced by this effect, as it measures the strength of the material and therefore less on the surface.

2.3.4 Conclusion

In this section the principle that the Leeb hammer and the Schmidt hammer use to asses concrete is explained. The rebound hammer and the Leeb hammer use the principle of energy loss due to plastic deformation relative to strain energy. The original rebound hammer relates the spring energy after the impact to the initial spring energy. The Silver Schmidt Hammer uses the relation between the kinetic energy before and after the impact. The Leeb hammer uses the same relation as the Silver Schmidt Hammer. The biggest difference between the Leeb hammer and the Schmidt hammers is the impact energy. The Leeb hammer uses a significantly lower impact energy. For low impact energies on materials with a high compressive strength the rebound method is expected to show a relation with the elastic modulus rather than the

compressive strength of the material. Contradictory is research showing a clear relation between the compressive strength and the Leeb hardness values, where mainly the age of the material influences the measured values. The relation between the velocity after an impact related to the velocity before the impact is however proven to be a solid method of determining the strength of the material. In section 2.2 was discussed how a void clearly influences the strength of the material and a crack has a diffuse relation to the strength of the material. The influence of the flaw on the strength will influence the rebound value, which can be used for the assessment of concrete with a robotic arm. In the next section will be discussed how this principle will be used.

2.4 Robotic assessment of concrete based on the rebound principle

In the previous section is explained how the rebound principle is used to asses the strength of concrete. This section will explain how this principle can be used by assessing concrete with a robotic arm, this in order to answer the following sub-question: **How can the rebound hammer principle be used to locate structural flaws with a robotic arm?**

In order to answer this question specifications of the robotic arm are given. Then there will be explained how to mimic the principle of the hammers with a virtual spring. How to implement a virtual spring by using impedance control will be explained. Accordingly how to estimate the external force applied on the end-effector will be explained.

2.4.1 Impact test with virtual spring

In order to mimic the principle of the rebound hammer, the energy loss to plastic deformation should be determined. A virtual spring will be placed at the end-effector, as shown in figure 2.26, which imitates the effect of the spring of the Silver Schmidt hammer. The mass of the robotic arm imitates the effect of the mass attached to the spring of the hammer.

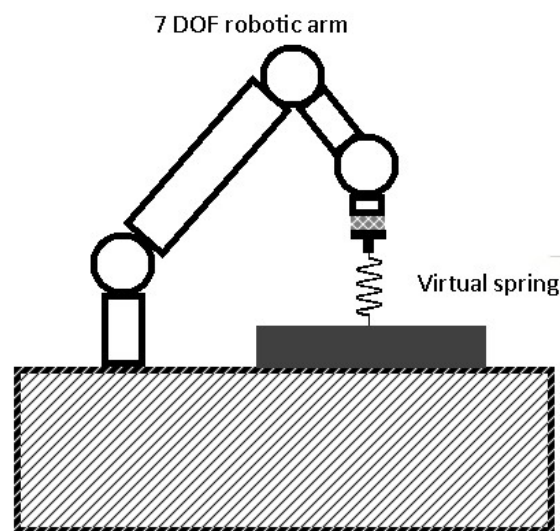


Figure 2.26: Overview of virtual spring attached to the end-effector of the robotic arm

The virtual spring instantly attached to the end-effector will cause the end-effector to be drawn towards the surface of the sample and impact the surface with a certain impact energy. Accordingly, the hammer will bounce back on the surface with a certain speed. Based on the velocity at impact and the velocity when bouncing the rebound value should be determined. This velocity response of the Leeb hammer is shown in figure 2.27 (Kovler et al., 2018a).

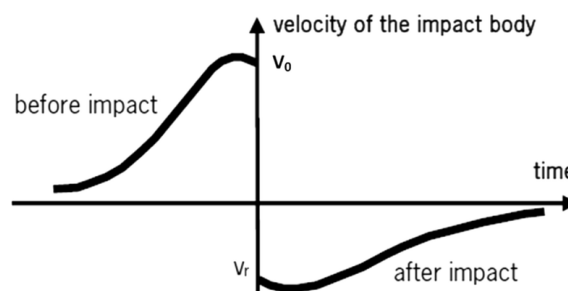


Figure 2.27: Velocity response of the Leeb hammer

A similar velocity response is expected when impacting with a robotic hammer and the rebound value will be determined based on the rebound velocity relative to the initial velocity. This rebound value relates to the compressive strength, which then again is related to cracks and voids in the concrete. Therefore it is expected that impacting a surface with a robotic arm can be used to determine a certain rebound value that is related to the relation between the elastic modulus and the compressive strength.

$$R = \frac{v_{\text{out}}}{v_{\text{in}}} \quad (2.11)$$

Where v_{out} is the maximal velocity of the end-effector after the impact and v_{in} is the velocity of the end-effector at impact. This is the same relation as used by the Leeb hammer, similar to the Leeb hammer, it is therefore assumed that the direction of impact with respect to the direction of the gravity has no considerable influence on the measured rebound value. Based on the analysis in section 2.2 the rebound value is expected to be lower in the case of flaws. Therefore it is expected that the impact with a robotic arm can be used to locate flaws based on the rebound value, where the rebound value can be used as relative measurements. An experimental study is however needed in order to determine whether this is actually the case.

In order to determine the rebound value, the velocity of the end-effector should be determined. This velocity can be determined based on the angular velocity of the joints. The relation between these velocities is shown in equation 2.12.

$$T_0^n = J(q) \cdot \dot{\theta}_n \quad (2.12)$$

Where T_0^n is the twist of the end-effector with respect to the base frame, where the velocity in the Cartesian frame can be determined based on the twist. $\dot{\theta}_n$ is a vector containing the measured angular velocities in the joints. $J(q)$ is the Jacobian, which depends on the configuration. The Jacobian will be explained in the next subsection.

As shown in section 2.3.2, the Leeb hardness not only depends on the yield strength, but also on the elastic modulus. Because this method will use the same impact principle, it is expected that a similar relation between the elastic modulus and the compressive strength will be measured. This could be tested by impacting on a material with a much lower elastic modulus, but a similar compressive strength, as a higher rebound value is expected for that case.

2.4.2 Jacobian

In order to determine the velocity of the end-effector in equation 2.12, the Jacobian has to be determined for each configuration. The Jacobian for a seven degrees of freedom serial robotic arm can be given by the following equation (Stramigioli and Bruyninckx, 2001).

$$J = [\tilde{T}^1 \quad \tilde{T}^2 \quad \dots \quad \tilde{T}^n] \quad (2.13)$$

Where J is the Jacobian and \tilde{T}^i is the twist of each joint. In this case the Jacobian does not include the effects of deflections of the links. In the case of a small deflection, the Jacobian has a small error. In that case the twist calculated in equation 2.12 also contains a small error. The magnitude of this error however depends on the deflection of the links. For this assessment method it is required to apply an impact on the surface and therefore a certain force on the robotic arm. The deflection of the links will depend on the stiffness of the links and the force applied. The deflections will however influence the estimations done during impact, while this is also the moment the rebound value should be estimated. Experiments in the experimental study should show if this effect is problematic in determining the rebound value.

2.4.3 Impedance controller

The virtual spring attached on the end-effector can be realized by using an impedance controller. A controller in the Cartesian frame can be simplified into the following equation.

$$\vec{F}_{\text{virtuallspring}} = -K\vec{e} - D\vec{\dot{x}} \quad (2.14)$$

Where $\vec{F}_{\text{virtuallspring}}$ is the force of the virtual spring-damper acting on the end-effector. K is the stiffness matrix, D is the damping matrix. \vec{e} is the error between the desired position of the spring and the position of the end-effector. $\vec{\dot{x}}$ is the velocity of the end-effector in the Cartesian frame. Based on the task force the task torques for the joints can be determined using the transpose of the Jacobian.

$$\vec{\tau}_{\text{virtuallspring}} = J(q)^T \vec{F}_{\text{virtuallspring}} \quad (2.15)$$

Where $J(q)$ needs to be transposed and $\vec{F}_{\text{virtuallspring}}$ is calculated in equation 2.14. $\vec{\tau}_{\text{virtuallspring}}$ is a vector containing the torques in each joint that represent the force applied by the virtual spring on the end-effector.

The stiffness matrix is determined based on the following equation.

$$K = \begin{bmatrix} K_{\text{translation}} & 0 \\ 0 & K_{\text{rotation}} \end{bmatrix} \quad (2.16)$$

Where the translation stiffness matrix and rotation stiffness matrix are three by three matrices. For simplified usage only the diagonals will be used. The stiffness matrix for translation can be formed by the following equation.

$$K_{\text{translation}} = I_3 \vec{k}_{\text{translation}} \quad (2.17)$$

Where $\vec{k}_{\text{translation}}$ is a vector of three elements, where each element represents a stiffness of a direction in the Cartesian frame. I_3 is an identity matrix (3x3).

$$\vec{k}_{\text{translation}} = \begin{pmatrix} k_x \\ k_y \\ k_z \end{pmatrix} \quad (2.18)$$

K_{rotation} is configured the same way as $K_{\text{translation}}$, but then depends on the desired stiffness for rotation. As the equations are similar, this will not be explained in the same detail as $K_{\text{translation}}$. The damping matrix, D , from equation 2.14, is configured the same way as the stiffness matrix, K , but different values can be used in order to add damping to the system. A generally used value for damping is $2\sqrt{k}$ for each direction, where k are the stiffness values used for the stiffness matrix.

The virtual spring energy depends on the configured spring distance and the spring coefficient, as the spring energy is given by the following equation.

$$E_{\text{spring}} = \frac{1}{2} C x^2 \quad (2.19)$$

Where in this case x is the initial distance between the end-effector and the spring position and C is in this case the stiffness matrix K . This means the impact energy can be determined with the spring distance and the spring stiffness. The maximal impact energy the assessment with a robotic arm can apply is however limited due to the fact that a too high impact can cause

damage on the robot itself. The actual impact energy that can be achieved with the robotic arm, can be determined based on the kinetic energy. The kinetic energy can be determined based on the mass of the links of the robot and the velocity of the joints, as shown in the following equation.

$$E_{\text{kin}} = \frac{1}{2} \vec{q}^T M(q) \vec{q} \quad (2.20)$$

Where \vec{q} is a vector of the velocities of the joints and $M(q)$ is the mass-matrix of the robot, which depends on its configuration. The impact that should be applied in order to locate structural flaws will be discussed in the experimental study in the next chapter.

In theory the spring distance and spring stiffness will only influence the impact energy. The spring distance and stiffness itself are not expected to influence the results. This should be tested by applying the same impact energies but with different distances and stiffness settings. Also the influence of damping should be revised. Damping is desired, as otherwise stability issues are to be expected, however added damping could influence the results. The robotic arm itself has also damping, due to friction. Looking at the influence of damping will also give an idea of the influence of the friction of the robotic arm. In case the influence is severe, compensation for friction can be considered as a solution.

2.4.4 Aspects to take into account when measuring with a robotic arm

As mentioned in section 2.4.2, inaccuracies on the measurements are expected due to deflections in the arm, while the stiffness of the arm will depend on its configuration. The stiffness of the arm is unknown and needs to be determined, accordingly the influence of the configuration on the rebound value needs to be determined via experimental data. The influence on the measured position and velocity of the end-effector is important, as the relation between the impact velocity and the rebound velocity are used to assess the concrete.

2.4.5 Conclusion

In this section is discussed how to locate structural flaws in concrete sewer pipes with a robotic arm by using a virtual spring in order to use the rebound hammer principle of the leeb hammer and the Silver Schmidt hammer, where the impact velocity can be related to the rebound velocity. This virtual spring can be made by using impedance control. In this section the equations for the impedance controller were shown and several variables were mentioned. The impact energy is expected to be of influence on the rebound value, as the impact energy seems to play a role of importance for differences between the Schmidt hammer and the Leeb hammer, as discussed in section 2.3.3. The maximal impact energy that can be applied on assessing concrete is however unknown, during the experimental study the maximal impact energy will be discussed. Furthermore it is important to investigate the accuracy of the velocity measurement of the end-effector, as this is used to determine the rebound value. In order to validate the assessment method test needs to be performed on a material with a different relation between elastic modulus and compressive strength, a concrete tile with a void and a concrete tile with a crack.

2.5 Conclusion of analysis

'To what extent can interaction between a robotic arm and the surface of a concrete pipe be used to locate structural flaws of the pipe?' In the analysis is determined that cracks and voids in concrete are selected as flaws that should be localized. These flaws show to lower the compressive strength of concrete. The compressive strength can roughly be determined by relating the rebound velocity to the impact velocity, which yields a certain rebound value. Instead of

determining this rebound value with a Schmidt hammer or Leeb hammer, this value could also be determined with a robotic arm by applying an impact on a surface and relating the rebound velocity to the impact velocity. The impact can be achieved by placing a virtual spring between the end-effector of the robot arm and the surface of the sample, by means of impedance control. In the next chapter an experimental study will be conducted in order to determine if this method can indeed be used to assess concrete.

3 Experimental Study

In the previous chapter the feasibility of locating structural flaws is analyzed. As mentioned, experimental study is required in order to determine if the rebound value of a sample can be determined properly with a robotic arm. In this chapter the proposed method to locate structural flaws will be tested, in order to answer the question: 'To what extent can interaction between a robotic arm and the surface of a concrete pipe be used to locate structural flaws of the pipe?'

First the design of the experimental setup will be explained. Secondly the different experiments that will be conducted will be mentioned. Then each experiment will be discussed separately, by explaining the experiment, showing its results and discussing the results. At the end of this chapter the overall results of the experimental study will be discussed.

3.1 Design of experimental setup

In this section the design of the experimental setup will be discussed. First an overview of the setup will be shown. Then the separate parts of the experimental setup will be mentioned and their specifications will be given.

3.1.1 Overview

In this section an overview of the experimental setup is given. A schematic overview of the experimental setup is shown in figure 3.1.

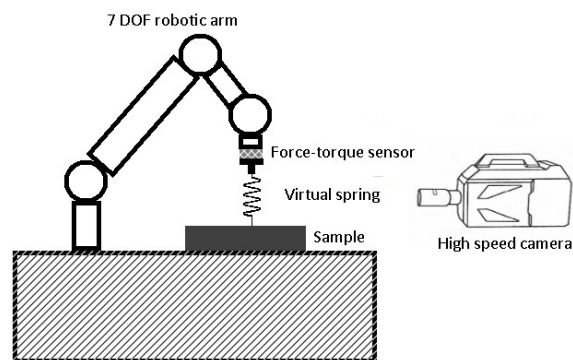


Figure 3.1: Schematic overview of experimental setup

The overview shows the design of the setup. Where a robotic arm with seven degrees of freedom, the Franka Emika Panda, is attached to a sample via a virtual spring. On the end-effector of the Panda a force-torque sensor is placed and a high speed camera is used to video the robotic arm, for which image processing will be used in order to validate the position estimation of the end-effector. A picture of the setup is shown in figure 3.2.



Figure 3.2: Picture of experimental setup

The picture shows the robotic arm with respect to the sample and the video camera. The camera is placed with a distance of 50 cm to the end-effector. One can also see the force sensor at the end-effector.

3.1.2 Robotic arm

For the experiments the 'Panda', manufactured by Franka Emika, will be used for the experiments. A picture of this robotic arm is shown in figure 3.3 ¹.



Figure 3.3: The Panda, manufactured by Franka Emika

The specifications of the panda are given in table 3.1. Additional specifications of the robot, like the dh-diagram and the contact limitations of all joints, can be found in appendix A.

Table 3.1: Panda specifications

Specifications	Value	Unit
Repeatability error	0.1	mm
Cartesian velocity limit	1.7	ms^{-1}
Cartesian acceleration limit	13	ms^{-2}
Degrees of freedom	7	
Communication rate	1	kHz
Maximum contact force	140	N
Payload	3	kg

As the table shows, the maximal contact force is 140 N. This is one of the limitations with regard to the maximal impact energy. Also the Cartesian velocity limit and the Cartesian acceleration limit should not be exceeded upon impact. Furthermore, the joint limitations shown in appendix A should also not be exceeded.

¹<http://donar.messe.de/exhibitor/hannovermesse/2017/X376456/product-brochure-eng-481544.pdf>

In order to control the robotic arm, an interface has to be used: The Franka Control Interface (FCI). A schematic overview of the communication between a workstation PC and the FCI is shown in figure 3.4 ².

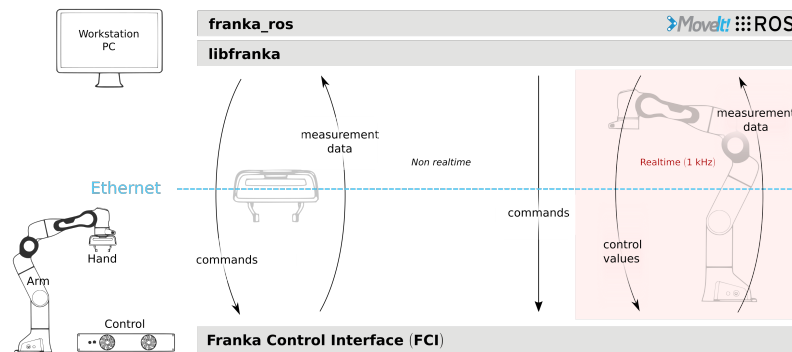


Figure 3.4: Schematic overview of Franka Control Interface

As the figure shows, communication can be achieved at a communication rate of 1 kHz. Commands have to be sent to the FCI and measurement data will be provided to the workstation PC. This measurement data includes measured torques in the joints and the angular position of the joints. The FCI does however also include a library which enables to receive the Jacobian at a certain configuration, the inertia matrix, the Coriolis and centrifugal vector and the gravity compensation torques. It also enables the external force estimation based on the measured torques, minus the Coriolis, centrifugal and gravity compensation, with a filter included. Instead of implementing functionality in order to estimate these values, the FCI library will be used to do so. The libfranka library is used to control the robotic arm. The available impedance controller is implemented by including the control into a cpp file. There has been chosen to use an impedance controller as this controller represents a virtual spring, which is used to mimic the spring used in all the rebound hammers.

3.1.3 Force sensor

In section 3.1.1 the use of a force-torque sensor is mentioned. This sensor is connected with screws on 3D-printed material, which is then connected to the robotic arm. The force sensor is used in order to validate the estimation of the external force applied on the end-effector. The force-torque sensor used is the Schunk mini-40-SI-80-4. In figure 3.5 ³ a picture of the force sensor is shown.



Figure 3.5: Schunk mini-40-SI-80-4

²<https://frankaemika.github.io/docs/overview.html>

³<http://sciencedocbox.com/Physics/75355109-Product-information-force-torque-sensor-ft.html>

The ROS package `netft_utils` is used to extract the data from the force sensor. The measurements will be biased into zero when attached to the robotic arm in order not to measure the gravity force applied on the material attached to the force sensor.

The external force applied on the end-effector can also be determined based on how the external force affects the torques of the joints. The external force acting on the end-effector can be determined by multiplying the inverse of the Jacobian with the external influence on the torques of the joints. In the case the Jacobian is not invertible, the pseudo-inverse of the Jacobian with the external influence on the torques of the joints should be used to determine the external force, which is shown in the following equation.

$$F_{\text{ext}} = J^\dagger \cdot \tau_{\text{ext}} \quad (3.1)$$

Where F_{ext} is the external force on the end-effector and J^\dagger is the pseudoinverse of the Jacobian. τ_{ext} is the external effect on the torques of the joints, which can be determined by the measured torque minus the effect of gravity, Coriolis and friction, as shown in the next equation.

$$\tau_{\text{ext}} = \tau_{\text{measured}} - \tau_g - \tau_{\text{Coriolis}} - \tau_{\text{friction}} \quad (3.2)$$

τ_{measured} is the measured torque, τ_g the torque in order to compensate gravity and τ_{Coriolis} is the influence of the Coriolis effect on the torque. This research will not go into depth how to determine these torques. Ott et al. (2004) shows how to determine the torque needed for gravity compensation, τ_g . Pigeon et al. (2013) shows how to determine the torque to compensate the Coriolis effect. With the values for these torques, τ_{ext} , the effect of the external force on the torques, can be determined. This can be used in order to determine the external force as shown in equation 3.1.

3.1.4 High speed camera

As mentioned in section 3.1.1 a high speed camera is used to validate the movement estimation of the end-effector. In this section the specifications of the high speed camera and the software used for image processing will be mentioned. The camera itself is shown in figure 3.6⁴.



Figure 3.6: Camera used for high speed filming, Nikon 1 j4

The shown camera is the Nikon 1 j4 and is placed 50 cm away from the point of impact. The camera can film in HD quality (1920x1080px) at 29.97 frames per second. The camera also has a slow motion feature, where it can film at 400 frames per second or 1200 frames per second for three seconds, the quality is decreased by a higher frame rate. 416x144px for 1200fps and 768x288 for 400fps. In figure 3.7 a frame of a video at a frame rate of 400 frames per second is shown and in figure 3.8 a frame of a video at a frame of 1200 frames per second is shown.

⁴/urlhttps://www.pinterest.ca/pin/368310075752504480/

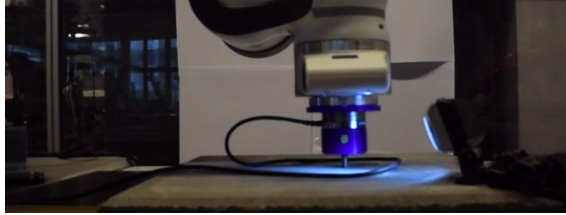


Figure 3.7: One frame from video of 400fps

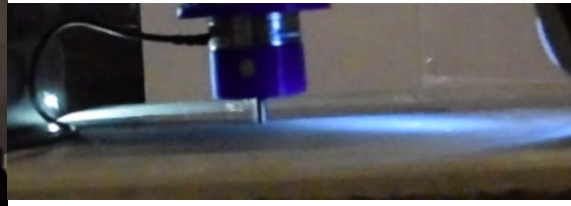


Figure 3.8: One frame from video of 1200fps

Both images show a clear difference in clarity of the image. The frame of the 1200 fps video shows the influence of the smaller resolution. The video of 400fps is therefore expected to measure the distance traveled by a point between two frames to be more precise. However also more time is passed between two frames with respect to the video of 1200 frames per second. Because of the resolution the impact will be captured with 400 frames per second. The captured video will be discussed and then it will be determined if 400 frames per second are enough to measure the impact velocity and the rebound velocity.

In order to determine the velocity of the end-effector based on the video, image processing is required. Kinovea image processing tool will be used in order to do so. The yellow dot on the blue printed plastic, visible in figure 3.7, for which the position will be determined. In order to relate the position in pixels to distance in meters, the length of the blue printed material will be used, which is 2.3 cm. In order to determine the velocity based on the position change over the frames, Kinovea has filtering included. The program uses two passes of a second order Butterworth filter; One forward and one backward, in order to reset the phase shift (Winter, 2009). Every point is extrapolated 10 points on each side in order to initialize the filter (Smith, 1989). The cutoff frequency is determined based on the estimation of the autocorrelation of residuals, by finding the frequency that yields the residuals that are the least autocorrelated. The filtered data set corresponding to this cutoff frequency is kept as the final result (Challis, 1999). The Durbin-Watson statistic is used to estimate the autocorrelation of the residuals. This filtering is a built-in feature of Kinovea and will be used as intended.

3.1.5 Virtual spring

Impedance control will be used to place a virtual spring between the sample and the end-effector. In this section the implementation of the impedance control will be described. Also the variables which will be used for the experiments are mentioned.

The impedance controller, mentioned in the analysis in section 2.4.3, is implemented in order to do an impact test. For the implementation has been chosen to further simplify the virtual spring in order to reduce the parameters for the tests. The impact will be applied in one direction only. A schematic representation of the virtual spring is shown in figure 3.9.

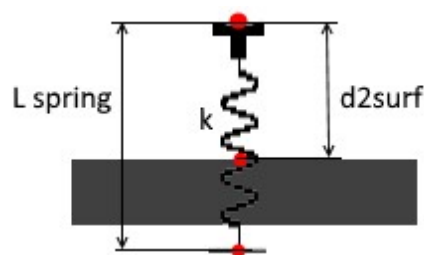


Figure 3.9: Schematic representation virtual spring

The figure shows two distances, the distance between the starting point and the surface, represented with d_{2surf} , from now considered as variable d_s , and the length of the spring, L_{spring} ,

as variable l_k . To test the feasibility of the method, there has been chosen to only test in the z-direction. The distances described in the figure are therefore one-dimensional. The distance between the surface and the starting point does not necessarily have to be equal to the length of the spring, as figure 3.9 shows. The relation between these distances can be described by the following equation.

$$r_d = \frac{l_k}{d_s} \quad (3.3)$$

Where l_k is the length of the spring, d_s is the distance between the starting point and the surface and r is the dimensionless value with represent the ratio between the two lengths. The variables which can be used to set the spring are d_s and r .

Figure 3.9 also shows the value k , which represents the stiffness of the spring. Equation 2.17 and 2.18 showed that a simplified impedance Cartesian impedance controller can be set with three stiffness properties, one for each direction.

$$\vec{k}_{translation} = \begin{pmatrix} k_x \\ k_y \\ k_z \end{pmatrix} \quad (3.4)$$

As the spring is simplified to be one directional, the stiffness that will influence the impact energy is k_z . The other stiffness properties, k_x and k_y are set very high, namely 5000 Nm^{-1} , so the impactor will be guided into being applied in one direction, which can be compared with the housing of a rebound hammer. k_z is a variable of the impedance controller that should be tuned for the experiments.

In section 2.4.3 is mentioned how the virtual spring energy can be determined. Because the virtual spring is simplified to the one dimensional case, the spring energy depends on the length of the spring and the spring stiffness. However, when the spring is placed under the surface of the sample, not all the spring energy will be converted into kinetic energy. The following equation represents the effective spring energy.

$$E_{\text{spring,eff}} = \frac{1}{2} k_z l_k^2 - \frac{1}{2} k_z (l_k - d_s)^2 \quad (3.5)$$

The impact energy is however the spring energy that is converted into the kinetic energy. The spring energy can also be lost due to friction before the impact is achieved. The kinetic energy at impact will be considered as the impact energy and can be determined based on the following equation, as mentioned in section 2.4.3.

$$E_{\text{kin,in}} = \frac{1}{2} \vec{q}_{in}^T M(q) \vec{q}_{in} \quad (3.6)$$

Where \vec{q}_{in} is the angular velocity of the joints at impact and $M(q)$ is the mass matrix.

3.1.6 Samples

In this section the samples used for the experimental study will be shown and be discussed. For the test concrete tiles will be tested. In figure 3.10 a photo of a concrete sample is shown. Two of these tiles were tested. In figure 3.12 two tiles with a difference in thickness are shown. One tile is 4.5 cm thick, the other 8.5 cm thick.



Figure 3.10: Concrete tile

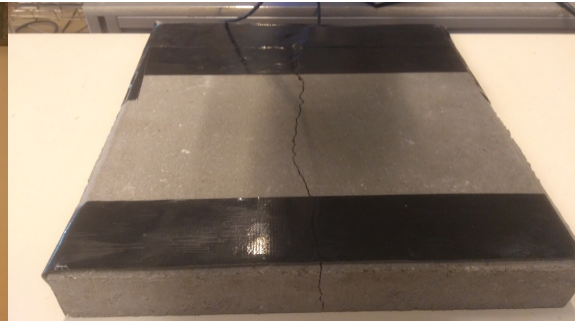


Figure 3.11: Concrete tile with a crack

On one tile, with the thickness of 4.5 cm, a crack has been induced, figure 3.11. Another tile, with the thickness of 8.5 cm has been damaged by making a void on the back of the tile, figure 3.13.



Figure 3.12: Two concrete tiles, 4.5 cm and 8.5 cm



Figure 3.13: Concrete tile with a void

For the tile with the void, the undamaged side will be tested in order to see the influence of the damaged side on the results. Also a rubber tile will be tested in order to see the influence of the elastic modulus on the rebound value. Both sides of this tile are shown, because the tile has a pattern on the back of the tile. The tile is shown in figure 3.14 and figure 3.15.



Figure 3.14: Upside of rubber tile



Figure 3.15: Downside of rubber tile

These samples will be placed on a table in order to induce an impact test on the sample. In figure 3.16 the placement of a sample on the table is shown, where the middle of the sample will be placed at a distance of 60 cm in y direction from the robotic arm.



Figure 3.16: Placement of sample with axis

3.1.7 Impact Test

In this section will be explained how the impact test will be conducted with the experimental setup. An activity diagram is shown in figure 3.17 on how the the test will be conducted.

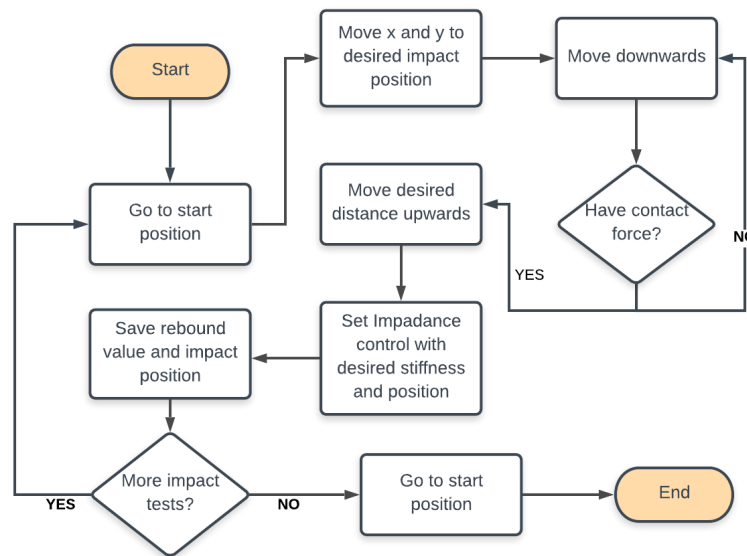


Figure 3.17: Activity diagram of impact test

The figure shows the various steps of the impact test. The rebound value for each impact test will be determined based on the rebound velocity divided by the impact velocity, as discussed in section 2.4. During the velocity response will be used in order to determine the rebound value. A velocity response that could be expected is shown in figure 3.18.

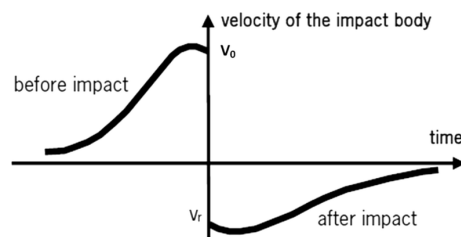


Figure 3.18: Expected velocity response of impact

The velocity response of the end-effector has to be determined based on the angular velocity of the joints.

3.2 Description of experiments

As concluded in the analysis, a variety of tests is required in order to determine if a robotic arm is able to locate structural flaws in concrete. In this section will be discussed which experiments will be conducted, based on the analysis.

3.2.1 Validation impact test

The design of the experimental setup explains how the robotic arm will be used to determine the rebound value. The goal of the first experiment is to validate the impact test. This will be achieved by determining the velocity of the end-effector based on the angular velocity of the joints and compare this velocity with the velocity measured with the high-speed camera. Then the rebound value will be determined for multiple tests on the same position in order to determine the variance of the rebound value test with a robotic arm. This rebound value and variance will be compared with a rebound value test with a Schmidt hammer on the same position as the robotic arm tested the rebound value.

3.2.2 Internal deflection robotic arm

As mentioned in the analysis, in section 2.4.1, deflection of the arm can influence the measured velocity. To analyze the performance of the impact test, it is therefore necessary to determine the influence of the stiffness of the arm on the measured value. Tests are required in order to determine the stiffness of the robotic arm. This is also required in order to relate this research to the use of other robotic arms.

When the stiffness properties of the robotic arm are determined, the influence of these stiffness properties on determining the velocity and the rebound value should be investigated. This can be achieved by comparing the velocity of the end-effector based on the measurements of the angular velocity of the joints with the velocity of the end-effector determined by the image processing of the video captured by the high speed camera for the different positions. A look will be given if the velocity estimated by the Panda is comparable with the velocity determined with the camera for each impact position.

3.2.3 Influence virtual spring settings on measured rebound value

In section 3.1.5 is explained how the impedance controller is implemented. The implementation showed two variables, d_s , the distance between the starting point and the surface of the sample, and r , the relation between the length of the spring and the distance to the surface. An experiment needs to be done in order to determine if these parameters influence the measured rebound value, without changing the spring energy. The experiment will be described in chapter 3.5. In section 2.3.3 is mentioned that impact energy can also influence the rebound value. It is therefore necessary to inspect the influence of the impact energy on the measured rebound value via the experimental study. Therefore a sample will be tested on the same position with different impact energies in order to determine the relation between the impact energy and the rebound value for the given experimental setup.

3.2.4 Influence of relation between elastic modulus and compressive strength on measured rebound value

As discussed in the analysis, in section 2.3, the rebound value shows a relation between the compressive strength and the elastic modulus. In order to show this effect, the impact test will be conducted on two materials with a big difference in elastic modulus. The experiment will be conducted on a concrete tile and also on a rubber tile and study the influence of the difference in material on the measured rebound value.

3.2.5 Localization of flaws

In order to determine the feasibility of locating structural flaws due to interaction with a robotic arm, it is necessary to study if the proposed impact test is able to locate structural flaws. An experimental study should be conducted in order to be able to determine if the impact test can be used to locate the structural flaws. This will be done by impact testing undamaged concrete tiles and impact testing damaged concrete tiles. Based on these tests there should be determined if it is possible to identify flaws. This will also give a indication if the flaws can be localized.

3.3 Validation of impact test

The goal of this experiment is to validate the impact test. In this section first the design of the experiment will be explained. Then the results will be shown. Accordingly the results will be discussed.

3.3.1 Design of experiment

In order to validate the impact test, the impact test will be applied on a concrete tile, as explained in section 3.1. The estimated velocity of the end-effector by the Panda will be compared with the velocity estimated by the high-speed camera. The impact test will be done with the variables shown in table 3.2.

Table 3.2: Variables of impedance controller

Variable	Value
k_z	250 N m^{-1}
r	1.25
d_s	0.04 m
$E_{\text{spring,eff}}$	0.3 J
x	0 m
y	0.6 m

The point of impact, $x = 0\text{m}$ and $y = 0.6\text{m}$, will also be the middle of the concrete tile. For the first impact test the vertical and horizontal velocity of the end-effector was measured with the high speed camera and measured with the velocity measured by the joints of the Panda. First the performance of the built-in filter of Kineovea will be analyzed. Then the velocity measured by the Franka will be shown. Accordingly the measurements by the Franka will be compared with the measurements of the camera. Based on the relation between the vertical impact velocity and the vertical rebound velocity of the end-effector the rebound value can be determined, as explained in section 2.4. This test will be done ten times, in order to determine the consistency of the test. Of this ten tests the mean and the deviation will be determined. Then the strength will be measured on the same spot with a Schmidt hammer. The mean and the deviation of the measurements of the rebound hammer will be determined based on ten measurements. In section 2.3 is mentioned that the rebound value of the Schmidt hammer does depend of the direction of the measurement with respect to the gravity. In section 2.4 is mentioned that the rebound value measured with the Franka does not depend on the direction with regard to the gravity. Therefore the rebound value measured with the Schmidt hammer will be converted to the rebound value of the Schmidt hammer that would be measured without influence of the gravity, based on the conversion graph in figure 2.17, shown in section 2.3.1. The mean and deviation of the converted rebound values of the Schmidt hammer will be compared with the mean and deviation of the rebound values measured with the robotic arm.

3.3.2 Results

This section will show the results of the impact test on a concrete sample. First the vertical and horizontal velocity of the end-effector measured by the camera will be analyzed. Then the estimation of the velocity by the Panda will be reviewed. The estimation of the Panda will be compared with the estimation of the camera. Then the rebound values, measured with the Panda and the Schmidt hammer, will be shown.

The position of the end-effector was measured with the high-speed camera at 400 frames per second. Based on the change in position between the frames, the velocity can be determined. In figure 3.19 the vertical velocity of the end-effector, measured by the camera is shown. In figure 3.20 the horizontal velocity of the camera is shown.

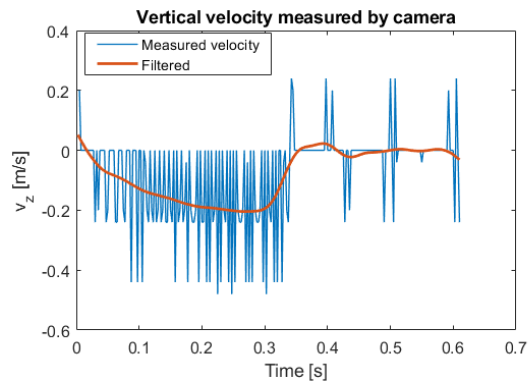


Figure 3.19: Vertical velocity of the end-effector measured by the camera

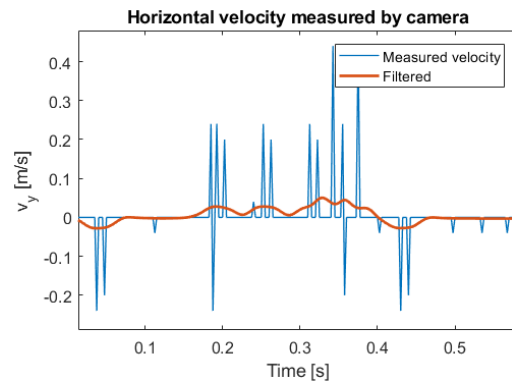


Figure 3.20: Horizontal velocity of the end-effector measured by the camera

The figure also shows the filtered velocity, which has been filtered with the built-in filters of 'Kinovea', as mentioned in section 3.1.4.

Also the Panda measured the velocity of the end-effector, based on the angular velocity of the joints. The vertical velocity is shown in figure 3.21 and the horizontal velocity is shown in 3.22.

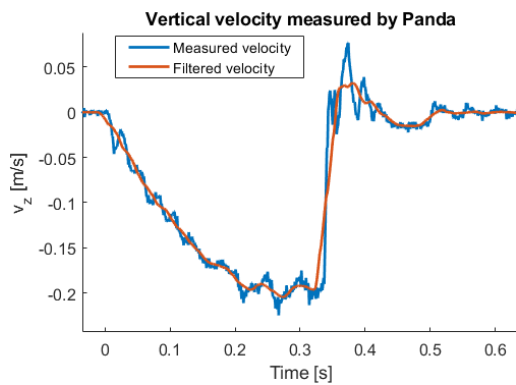


Figure 3.21: Vertical velocity of the end-effector measured by the Panda

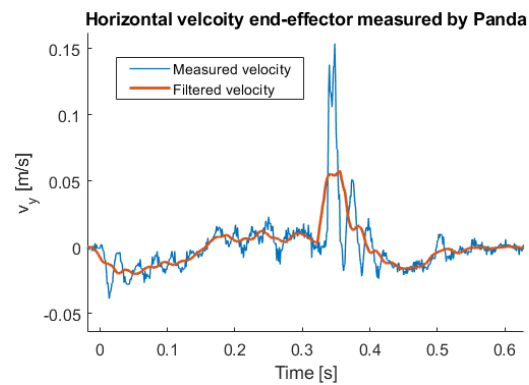


Figure 3.22: Horizontal velocity of the end-effector measured by the Panda

Also this velocity is filtered, as the velocity seems to show some noise. The signal was filtered with a moving average filter with a window of fifteen samples.

In order to validate the velocity measured by the Panda, the estimated velocity needs to be compared with the velocity measured with the camera. Figure 3.23 shows the vertical velocity of the end-effector and figure 3.24 shows the horizontal velocity of the end-effector.

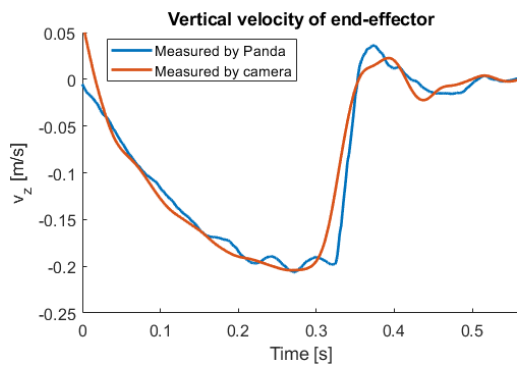


Figure 3.23: Vertical velocity of the end-effector

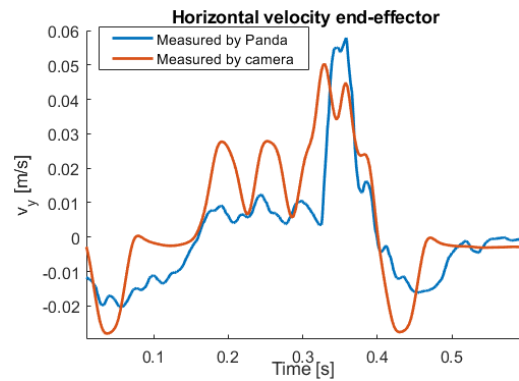


Figure 3.24: Horizontal velocity of the end-effector

In order to be able to see the characteristics of the velocities, there is chosen to not use the same scale on the velocity axis.

In figure 3.25 the position of the end-effector is shown.

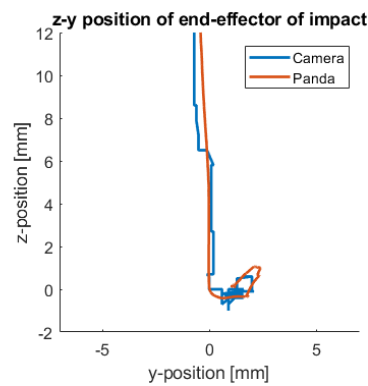


Figure 3.25: Vertical position versus the horizontal position

Based on the relation between the vertical impact velocity and the vertical rebound velocity of the end-effector, the rebound value of an impact can be determined. This is done for ten measurements, from which the mean and the standard deviation are determined. This is also done for ten rebound measurements with the Schmidt hammer. The measurements are compared in figure 3.26.

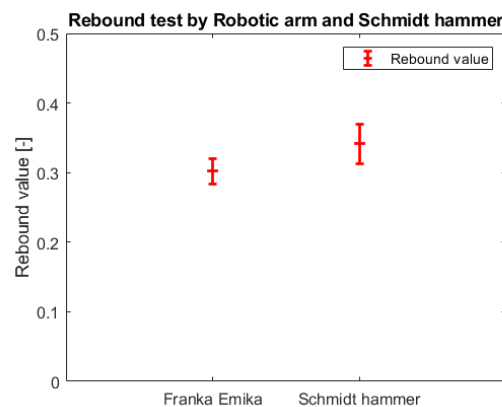


Figure 3.26: Rebound value of robotic arm compared to rebound value of Schmidt hammer

3.3.3 Discussion

In this section the results of the experiments are discussed in order to validate the impact test. Figure 3.19 and figure 3.20 show the need for the filtering. Also the measured velocities of the Panda, figure 3.21 and figure 3.22, need some filtering due to high frequent noise. Filtering of the high frequent behavior is desired, as the principle of the Schmidt hammer and the Leeb hammer is used to determine the strength of the material. These hammers use the low frequent dominant behavior and do not use any high frequent behavior of the impact. The two methods of measuring the velocity, the panda and the camera, are compared in figure 3.23 and figure 3.24. The two estimations clearly show similar behavior. It is interesting to see that for both estimations the end-effector shows quite some horizontal velocity after the impact. This is also visible in the yz-position of the end-effector in figure 3.25. It is not desired for the impact test to achieve a horizontal velocity, as this velocity is not perpendicular to the surface and therefore not expected to be achieved by the impact. A look on a high speed video of the impact from a bigger distance showed the origin of this effect. One frame of this video is shown in figure 3.27 in order to explain the effect.

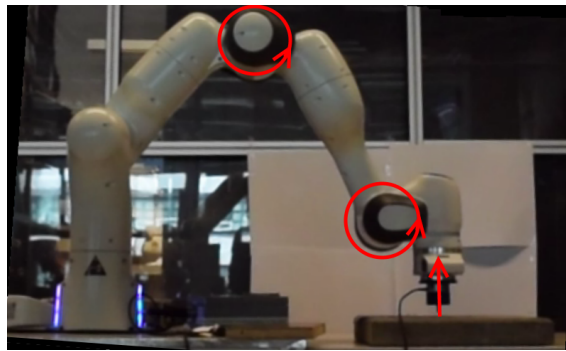


Figure 3.27: Explanation for horizontal displacement after impact

The reaction force of the concrete on the end-effector, shown with the red arrow in the figure, causes a deflection in the two joints that are red encircled. This results in a rotation around the axis of these joints, which gives a horizontal and vertical movement of the end-effector. Because the assessment method is a relative measurement method, the rebound velocity can still be compared with the impact velocity in order to obtain a rebound value.

Figure 3.26 shows the mean of the rebound value on a concrete tile of ten tests and the deviation of these ten tests. This is compared with a measurement with the Schmidt hammer, N-type, which has an impact energy of 2.2J. The impact on the concrete of the Schmidt hammer did actually slightly damage the surface of the concrete. The rebound values of both measurement techniques are actually quite similar for this setup. This can however not be used to relate the rebound value determined by the impact test with the robotic arm to the rebound value obtained by the Schmidt hammer, as it unknown if the relation is linear. A comparison study on concrete with different strengths and properties could be done in order to determine if there is a clear relation between the measurements with the panda and the measurements with a Schmidt hammer. It can be noticed that the deviation of the measurement with the Schmidt hammer is larger than the measurement with the Franka Emika. This could be the case, because an inexperienced user did the measurements with the device. Less deviation of the measurement method is a real pro, as less deviation in the measuring method means the method can be used to measure smaller deviations of the sample.

3.4 Influence of internal deflection of the robotic arm on measurements

In this section experiments on the influence of the internal deflection on the measured rebound value will be discussed. Because the stiffness properties of the Panda are not known, they will be determined for different positions. Then the robotic arm will conduct an impact test on several positions.

3.4.1 Design of experiment

The goal of this experiment is to determine the influence of the internal deflection of the robotic arm for different configurations on the determined rebound value.

In order to do so, first the internal deflection of the robotic arm will be determined. Then the rebound value will be determined for different positions.

In order to determine the stiffness of the robotic arm the deflection of the arm will be measured while the arm applies a slowly increasing force on a concrete tile. In section 2.2.4 is shown that the deflection of the tile is approximately zero when applying a point load of 50 N on a concrete tile. The measured deflection will therefore only be internal deflection of the robotic arm. The force measured by the robotic arm will be validated using an external force-torque sensor. The position of the end-effector will be validated with image processing of a video recorded by the Nikon j4, in order to show that the end-effector does not move when applying a force on the concrete tile. The difference between the measured position and the actual position shown on the camera relative to the force applied can be used to determine the stiffness. The accuracy of the measurement of the camera is considered to be 0.1 cm, based on small movements of 0.1 cm measured of a non-moving object. An accuracy of 0.1 cm is good enough for this test, as the accuracy of the Panda is also 0.1 cm. This will be done for three positions, at a distance of 50 cm, 60 cm and 70 cm in y position from the base of the robotic arm.

To determine the influence of the stiffness on the rebound value, an impact will be applied on 5 different positions on a concrete tile. The velocity of the end-effector determined by the Panda will be compared to the velocity measured with the high-speed camera. The variables of the impedance controller for the impact tests are shown in table 3.3.

Table 3.3: Variables of impedance controller

Variable	Value
k_z	250 N m^{-1}
r	1.25
d_s	0.04 m
$E_{\text{spring,eff}}$	0.3 J
x	0 m
y	50 cm, 55 cm, 60 cm, 65 cm and 70 cm

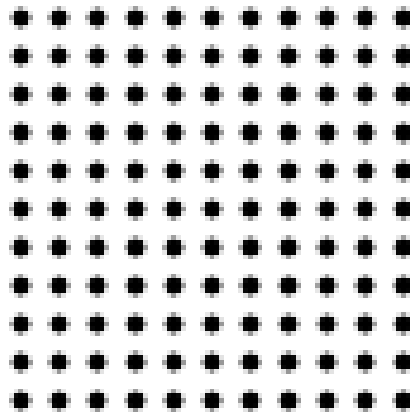
Each position impact test will be done ten times, in order to compare the rebound values on each position and determine the deviation of each test. This tests however assumes that the rebound effect of the material should be equal for each position. It can however be the case that certain parts of the tile yield other values. Therefore the same test will be also conducted a second time on the tile, but the tile will be rotated 180° around its z-axis. These two tests will also be done on a different concrete tile, in order to show that the measured behavior does not depend on the behavior of the single concrete tile.

In order to see the rebound value for different positions in the xy-plane, the impact test will be conducted on different xy-positions. The variables are shown in table 3.4.

Table 3.4: Variables of impedance controller for obtaining grid measurement

Variable	Value
k_z	250 N m^{-1}
r	1.25
d_s	0.04 m
$E_{\text{spring,eff}}$	0.3 J
x	-10 cm to 10 cm
y	50 cm to 70 cm

The x and y values will be used in steps of 2 cm. This will create a grid, where an impression of the impact positions is shown in figure 3.28.

**Figure 3.28:** Grid of impact positions

Based on the rebound value on each dot, a grid of the measured rebound values can be made. In case the configuration has a clear influence on the rebound value, one would expect a certain pattern on the grid caused by the influence of configuration. In order to determine the consistency, the test is done twice.

3.4.2 Results

In this section the results are shown of the experiments mentioned in section 3.4.1. In figure 3.29 the position of the end-effector is shown, based on the angular position of the joints, during the press test. This is compared with the position of the end-effector determined with the camera. In figure 3.30 the force applied on the concrete tile is shown. The force is determined based on the measured torques in the joints, but also measured with the force-torque sensor. Both are shown in the figure.

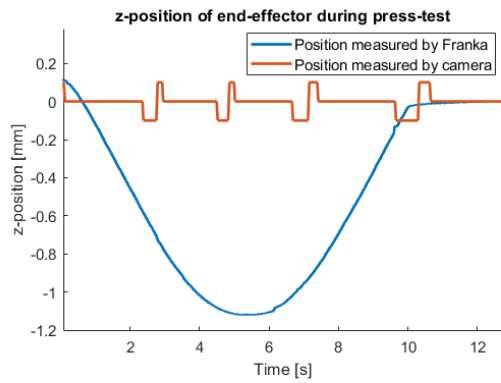


Figure 3.29: Position of the end-effector while applying a load on a concrete tile

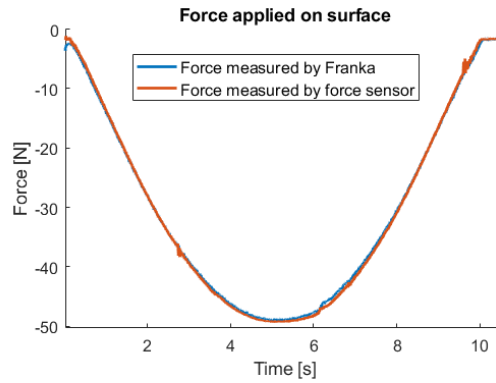


Figure 3.30: Force applied on concrete tile during press test

Accordingly the positions determined by the Panda while pressing on five different positions are shown in figure 3.31. The forces applied by the robotic arm are shown in figure 3.32.

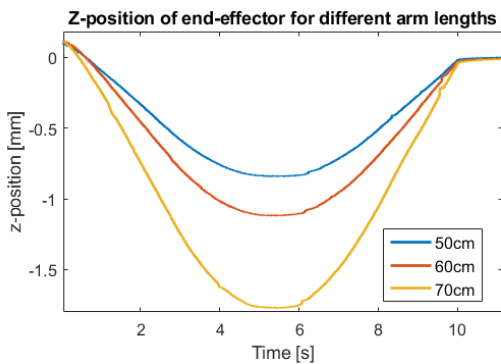


Figure 3.31: Position of the end-effector while applying a load on different positions

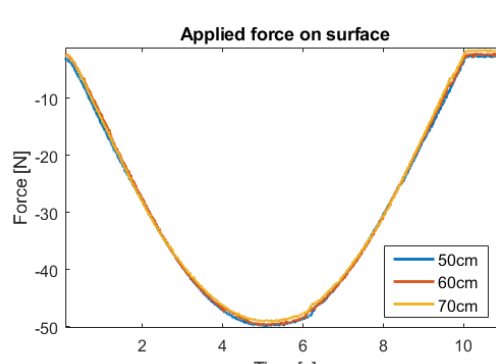


Figure 3.32: Force applied different positions

In figure 3.33 and figure 3.35 the vertical velocity response of an impact test at a distance of 50 cm and 70 cm is shown.

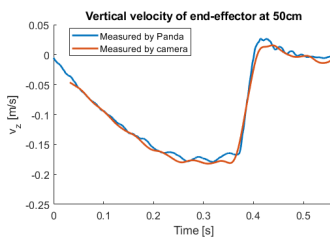


Figure 3.33: Vertical velocity of the end-effector at 50 cm

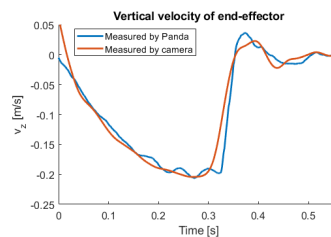


Figure 3.34: Vertical velocity of the end-effector at 60 cm

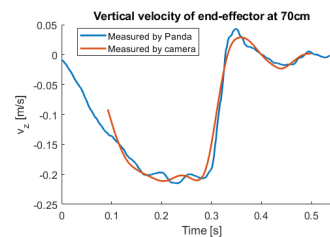


Figure 3.35: Vertical velocity of the end-effector at 70 cm

Under the assumption that the rebound value for the whole tile should be equal, in figure 3.36 the influence of the configuration on the rebound value is shown. In order to rule out the effect of the tile, the test is conducted twice. The deviation of the second test is shown in figure 3.37.

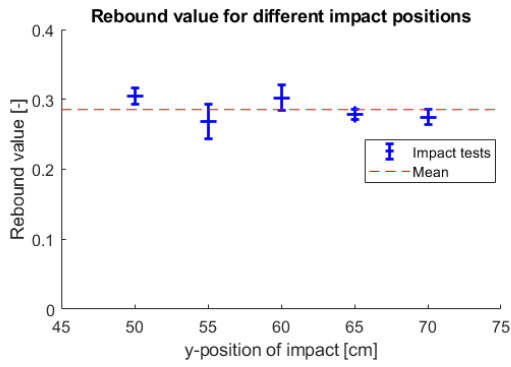


Figure 3.36: Impact position versus measured rebound value

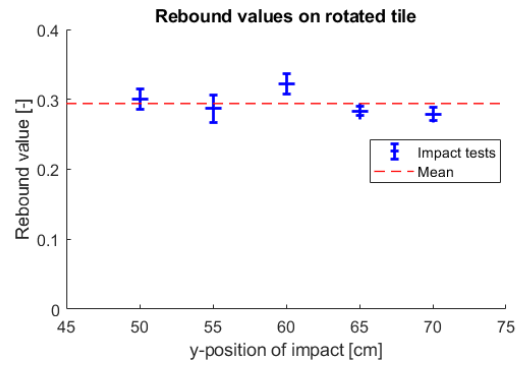


Figure 3.37: Impact position versus measured rebound value

In figure 3.38 and figure 3.39 the results of the same experiment are shown, but then on a different concrete tile. Again for the second figure, figure 3.39, the tile is rotated 180 degrees.

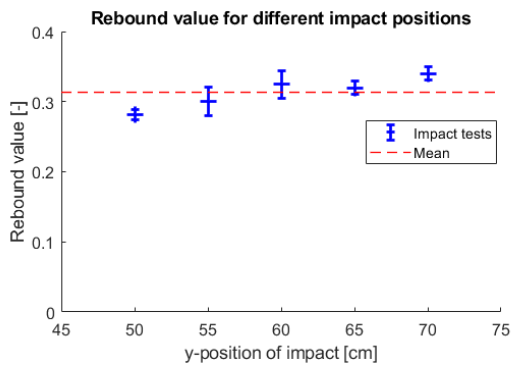


Figure 3.38: Impact position versus measured rebound value on other concrete tile

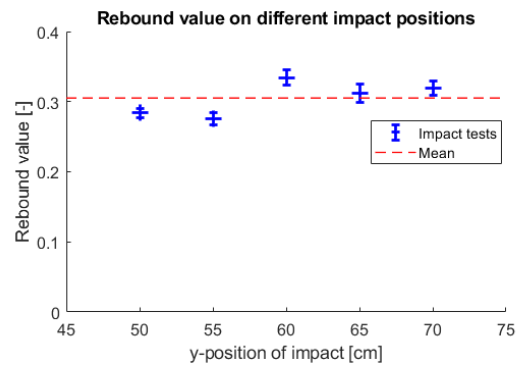


Figure 3.39: Impact position versus measured rebound value on other concrete tile

In figure 3.40 the rebound values of impact tests on different positions on the tile are shown. This test has been performed twice on the same tile, in order to show that it is repeatable.

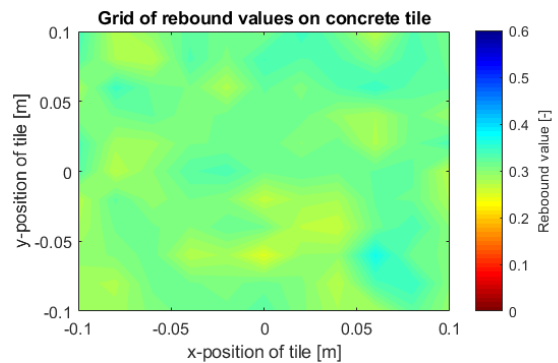


Figure 3.40: Rebound values on concrete tile

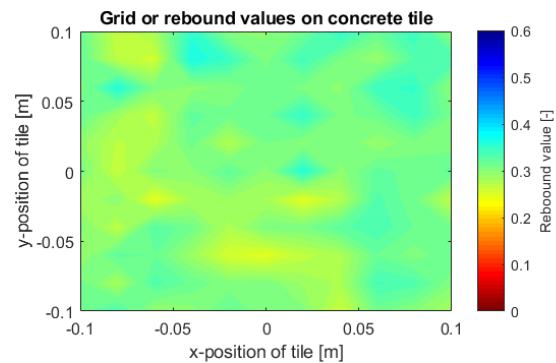


Figure 3.41: Rebound values on same concrete tile

3.4.3 Discussion

In figure 3.29 the position change of the end-effector in z-direction is shown for pressing on the middle of the tile. In the analysis, in section 2.2.4, was shown that close to no deflection is expected on a concrete tile while pressing with 50 N is to be expected. The footage of the camera actually shows some small bumps while pressing, but this is within the accuracy of the

measurement. The accuracy of the Franka can also be seen in the figure, as there is a difference of 0.1 cm between the start and the end of the measurement in the position measured by the Franka. The force applied on the surface, measured by the Franka is however almost the same as the force sensor measured. It seems that the deflection does not have a considerable effect on the force.

Figure 3.31 shows that the deflection really differs for different arm lengths. For a distance of 70 cm the deflection is 1.6 mm which is about twice the deflection when pressing on a distance of 50 cm. Again this has almost no influence on the measured force. It also seems that it has no influence on the measured velocity with the Panda compared to the measured velocity with the camera, shown in figure 3.33, 3.34 and 3.35. It is peculiar that all measurements show that the Panda measures a higher vertical rebound velocity than is measured with the camera.

In figure 3.36 the rebound value for a impact test on a concrete tile on different y-positions is shown. The rebound value on each position is quite close to the value of the overall mean. The position of impact and the measured rebound value do not show a clear relation. Figure 3.37 shows a similar behavior of the mean of the measured rebound value as figure 3.36. Also the mean on each impact position seems to be quite similar. This is however not as expected. The mean and the deviation at 50 cm of the first test should be similar as the mean and deviation at 70 cm of the second test, as those impacts are on the same point of the tile. Figure 3.38 and figure 3.39 are the impact tests on a different tile. Comparison of these two figures, again shows dependency on the impact position. For these two tests the dependency seems to be very different than the dependency of the first two tests. A clear relation between the impact position and the rebound value can therefore not be shown.

In both figure 3.40 and figure 3.41 a grid of rebound values on a concrete tile is shown. Comparing both figures shows that the deviation mentioned earlier is also present in these figures. Both tests show a small variation over the whole grid of the tile. It is also interesting to see that the grid shows similar marks on the tile for various areas. These areas are encircled in figure 3.42.

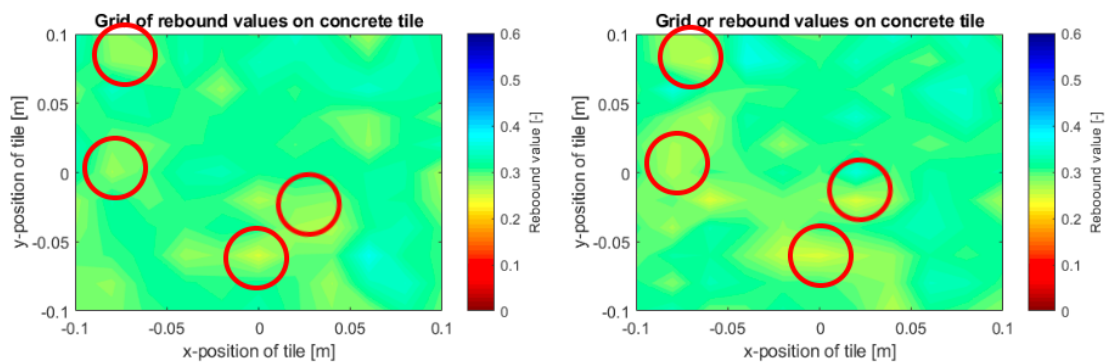


Figure 3.42: Similar areas

One would however expect that not only small areas coincide, but both whole figures coincide. That this is not the case, clearly has to do with the variation of the impact measurement, as both measurements were gathered the same way. Extracting the values of the second grid from the first grid, gives the figure shown in figure 3.43.

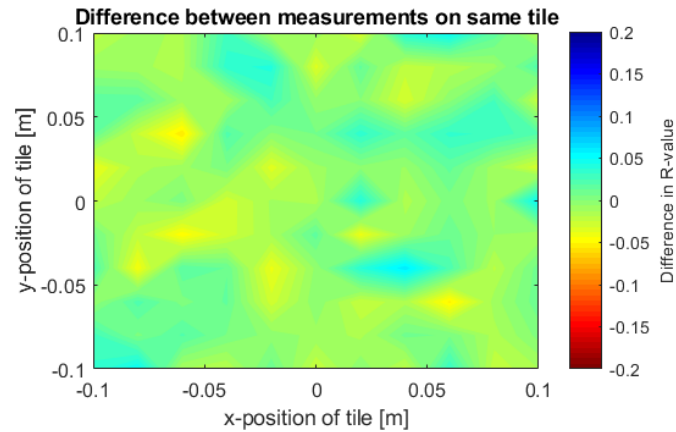


Figure 3.43: Difference between measurements on same tile

A clear influence of the deviation of the measurements can be seen, as no deviation would mean the value of zero everywhere. While these measurements show the influence of the variance of the grid of the rebound value, it cannot be determined if this deviation is to acceptable for its purpose. As the method is designed to locate flaws, not to determine if two tiles are identical. Future experiments should determine if the variance is acceptable. However, these experiments should be done with care with regard to the variance, as the variance is large.

3.5 Influence of spring settings on impact measurements

In this section the influence of the spring settings on the impact measurement will be investigated. In section 3.1.5 the different variables for implementation of the virtual spring are mentioned. In this section the influence of the distance to the surface, the length of the spring and the stiffness of the spring on the measured rebound value will be investigated.

3.5.1 Design of experiment

The goal of this experiment is to determine the influence of the spring settings on the measured rebound value. The different settings are the length of the spring, the distance to the surface and the spring stiffness.

In order to determine the influence of the parameters, an impact test will be done on a concrete tile on a single position with different spring settings. First a difference in the relation between the distance to the surface and the spring position will be tested for different distances, while keeping the spring energy constant. 3.5

Table 3.5: Variables of impedance controller with different spring settings

Variable	Value
r	1, 1.25 and 1.5
d_s	0.03 m, 0.04 m, 0.05 m, 0.06 m and 0.07 m
$E_{\text{spring,eff}}$	0.3 J
x	0 cm
y	60 cm

For the different settings the rebound value will be shown. Each test will be performed five times, in order to show the mean of each combination of settings. In theory the variables should not influence the rebound value, as the variables should not change any relation shown in the analysis. The experiments will make clear if this is indeed the case.

In section 2.3 the influence of the impact energy on the measured rebound value has been discussed. In order to see the influence of the impact energy on the rebound value, tests will be done with different virtual spring energies for a certain distance and position settings. The variables are shown in table 3.6.

Table 3.6: Variables of impedance controller with different spring stiffness

Variable	Value
r	1.25
d_s	0.04 m
k	110 N m^{-1} to 350 N m^{-1}
x	0 cm
y	60 cm

Where k is set in steps of 10 N m^{-1} , which gives a total of 25 experiments. All these experiments will be conducted six times, which gives a total of 150 impact tests. With these experiments a look will be given to the influence of the impact energy on the measured rebound value. As can be seen in the two conversion figures in section 2.3.1, the rebound hammer with a higher impact energy yield a lower rebound value. Therefore it is expected that for this test a higher impact energy will result in a higher rebound value.

3.5.2 Results

In figure 3.44 the influence of different spring properties on the measured rebound value is shown. Each point is the mean of five measurements. During evaluation of the experiments it appeared that the impact energy was not the same for each experiments, while the spring energy was the same for each distance. In figure 3.45 the applied impact energy is shown for each spring setting, where again, each point represents the mean of five measurements. The rebound value for the distance of 0.06 m and 0.07 m is zero, because no contact was made for these distances.

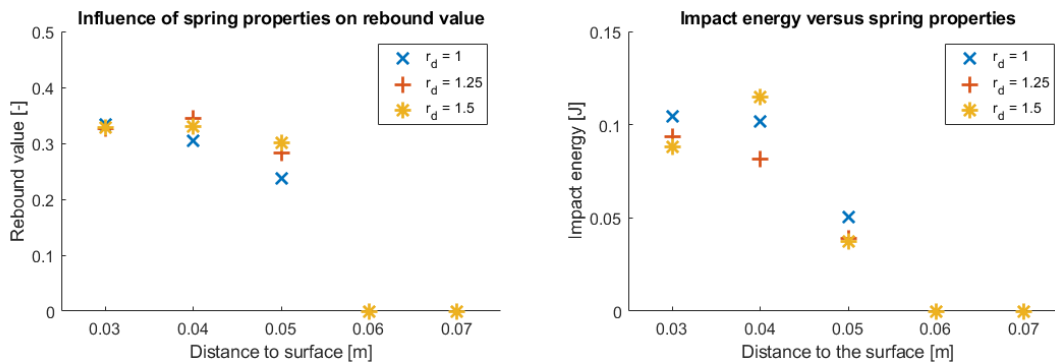


Figure 3.44: Relation between the virtual spring properties and the measured rebound value **Figure 3.45:** Relation between the virtual spring properties and the applied impact energy

In figure 3.46 the rebound value is related to impacts with different impact energy. The difference in impact energy is achieved by doing impact tests with different values for the stiffness.

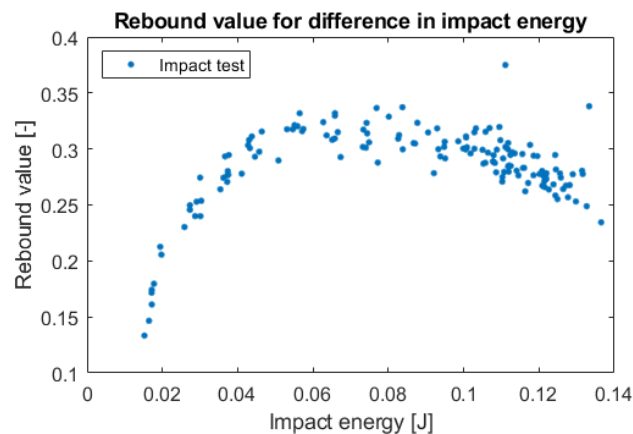


Figure 3.46: Rebound value related to difference in impact energy

3.5.3 Discussion

In figure 3.44 it can be seen that the rebound value for a impact test with a distance of 0.05 m is slightly lower than for the tests with shorter distances. In figure 3.45 can be seen that for this distance the impact energy is significantly lower, which could be a possible explanation the difference in rebound value.

For larger distances there is even no contact. As all tests are done with an virtual spring energy of 0.3 J, clearly not all energy is converted into kinetic energy. As the energy loss is larger for larger distances it is expected that a lot of energy is lost due to friction. The results show that the impact test should not be done with too large distances in the case friction is not compensated. Additional tests could be done with compensation for friction, in order to see if the impact

energies will be the same. This will however not be part of this research, in future experiments the distance to the surface will be set at 0.04 m.

It was not expected that r_d would have an influence on the rebound value. It appears that for a distance of 0.05 m the rebound value is quite lower for $r_d = 1$. What causes this difference is not clear. It does however seem that putting the other end of the spring at the surface does influence the results. Future experiments will be done with a r_d of 1.25.

Figure 3.46 shows the relation between the rebound value and the impact energy. For low impact energies the rebound value seems to increase. For higher impact energies the rebound value does show an decreasing rebound value for an increasing impact energy. For the low impact energies it is possible that actually no relation between the plastic deformation and the elastic deformation is represented, as maybe no plastic deformation is induced for such low impact energies. This can however not be proven. The graph also shows two dots which are really out of place, these are considered as measurement errors, in case this method is to be used there should be investigated if these errors happen more often and what causes them. Similar to earlier experiments, this experiment again shows a lot of deviation between the measurements. The decrease of rebound value for higher impact energies is not as expected, as mentioned a higher rebound value was expected for a higher impact energy. Additional research in future studies is required to determine the relation between the impact energy and the rebound value.

3.6 Influence of elastic modulus on impact measurement

In section 2.3.2 is mentioned how the elastic modulus influences the rebound value. It shows how the rebound value is related to the elastic modulus and the compressive strength, where a lower elastic modulus is expected to yield a higher rebound value. The goal of this experiment is to show the influence a different elastic modulus on the rebound value.

3.6.1 Design of experiment

In order to show the influence of the elastic modulus, the impact test will be conducted on concrete and on a material with a much lower elastic modulus, rubber, which is shown in section 3.1.6. In order to show the difference between the samples, the impact test will be applied on five different y-positions on the tile, 50 cm, 55 cm, 60 cm, 65 cm and 70 cm from the base of the robotic arm. This will be done for the concrete tile and the rubber tile. The mean and the deviation for each position will be shown. The material properties of the two samples are shown in table 3.7, which were mentioned in section 2.2.

Table 3.7: Variables of impedance controller with different spring stiffness

Variable	Concrete	Rubber
Y	30 GPa	0.05 GPa
$f'ck$	40 MPa	7 MPa

where Y is the youngs modulus and $f'ck$ is the compressive strength. After the test on the different y-positions, a grid test, similar to the test done in section 3.4, will be conducted on the concrete tile and on the rubber tile. On the rubber tile this test will be done a second time, in order to show the consistency. This second test will be done on a different rubber tile.

3.6.2 Results

In this section the results of the designed tests will be shown. First the velocity response of a single test will be shown. Then the results for the experiment on the various y-positions will be shown. Lastly, the several grid test results will be shown. Based on the kinetic energy on impact, the impact energy has been determined. This appeared to be 0.1J, which is similar to section 3.5. In figure 3.47 the velocity response during an impact on concrete is plotted against the velocity response during an impact on rubber.

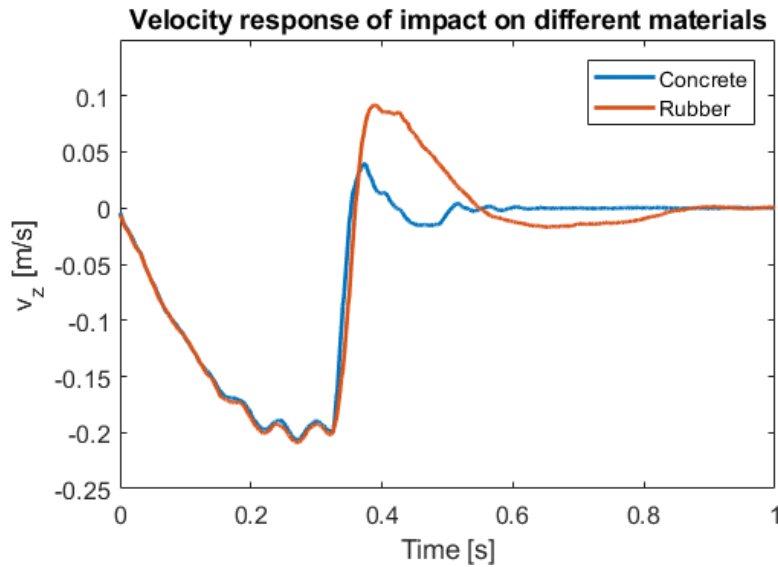


Figure 3.47: Velocity response on rubber versus response on concrete

Figure 3.48 shows the difference in rebound value for impact tests on a concrete tile and a rubber tile.

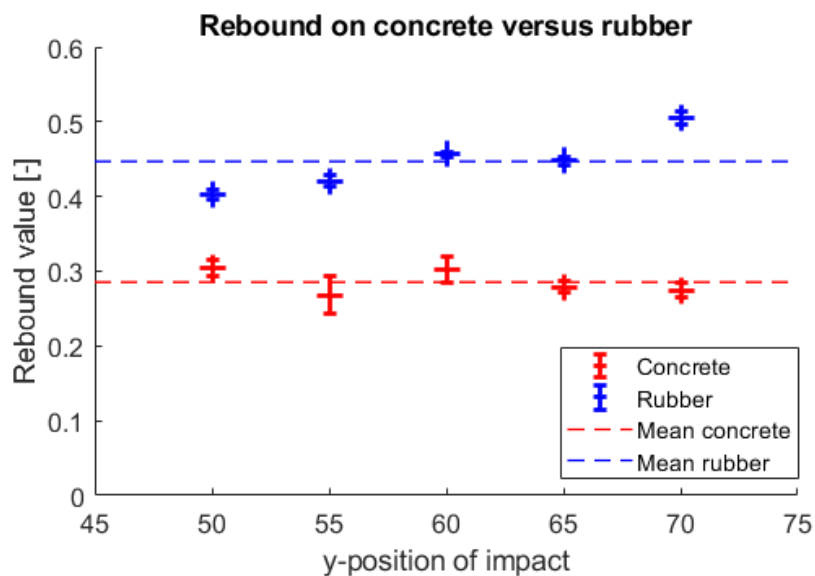


Figure 3.48: Rebound values for different impact positions for concrete compared with rubber

Accordingly the grid test on concrete has been performed, the grid is shown in figure 3.49. Figure 3.50 shows the grid obtained from the grid test on a rubber tile.

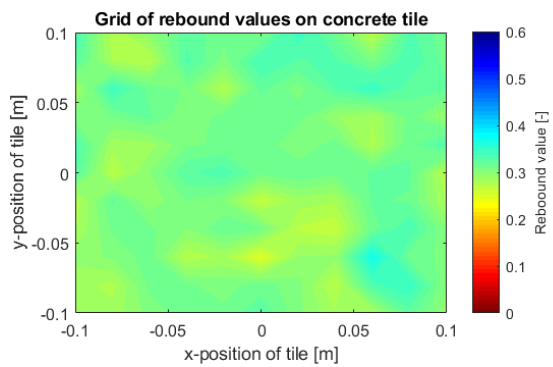


Figure 3.49: Grid of rebound values on concrete

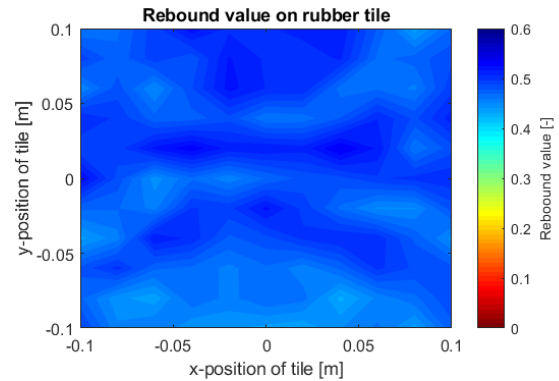


Figure 3.50: Grid of rebound values on rubber

As mentioned, the grid test on rubber is performed a second time, this result is shown in figure 3.51.

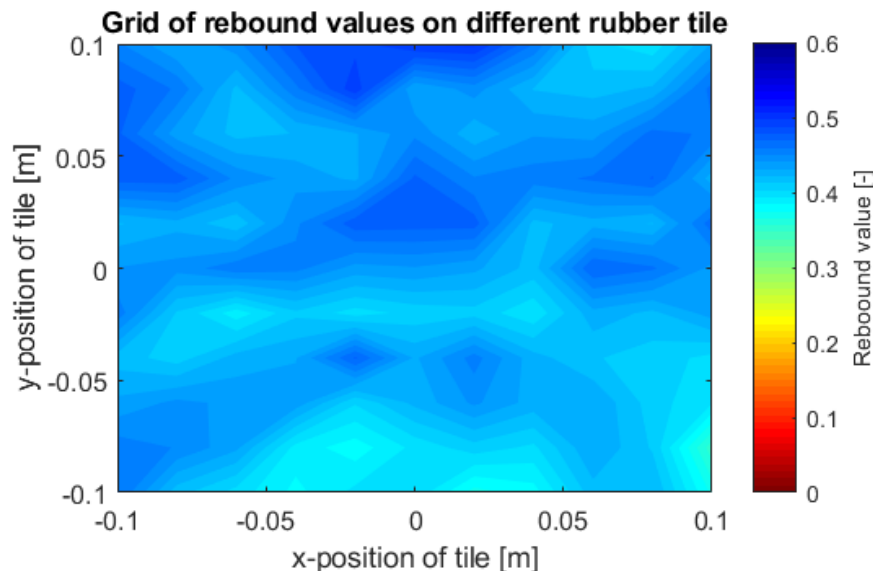


Figure 3.51: Grid of rebound values on different rubber tile

3.6.3 Discussion

The goal of this experiment is to show that an impact on a material with a lower elastic modulus will yield a higher rebound value. In figure 3.47 the velocity response of rubber is noticeable higher, which represents a higher rebound value. Figure 3.48 shows that this is higher rebound value is also measured for different positions. For both the concrete tile and the rubber tile, the deviation is significantly smaller than the difference measured between rubber and concrete. It is therefore safe to say that on rubber a higher rebound value will be measured on rubber than on concrete. This is in line with the expectation, as rubber has a lower elastic modulus. This lower elastic modulus results in a higher energy stored into strain energy relative to the plastic deformation, as mentioned in section 2.3.2. Based on these results can however not be concluded if this is also the case for other measurement methods, especially in case of a significantly different impact energy, which was for this experiment about 0.1 J.

In figure 3.50 the grid of rebound values of the grid test on rubber is shown, it is clearly different then the grid shown in figure 3.49, which is in line with the other results on the rubber tile. It is interesting to see a pattern shown in the figure of the rubber tile. This pattern shows similarity to the pattern shown on the back of the tile, which is shown in figure 3.52

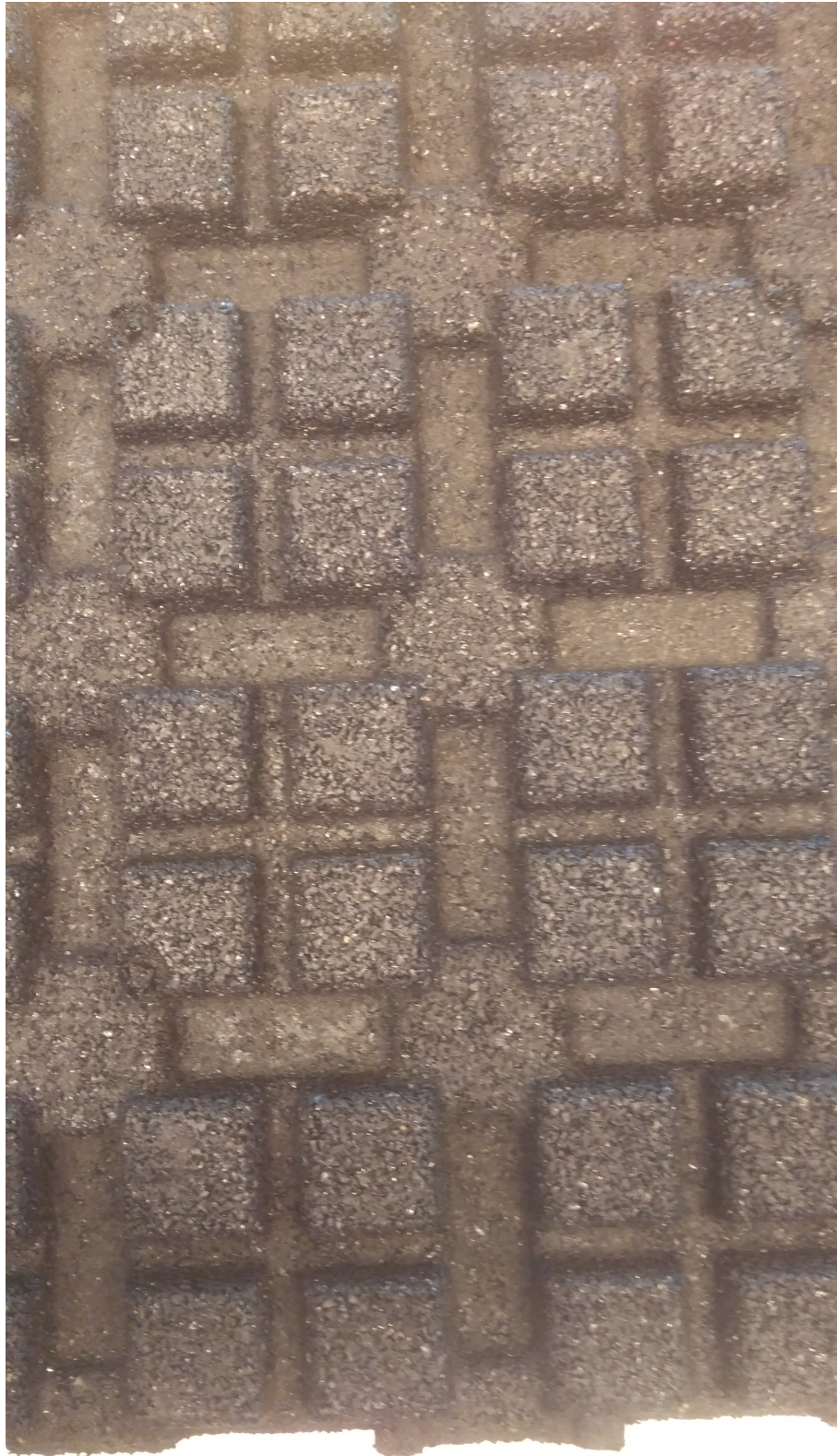


Figure 3.52: Pattern on the back of the rubber tile

The result on the other rubber tile, shown in figure 3.51, are quite similar as the result on the first rubber tile. It seems however that the rebound value over the whole tile is a bit lower than the first tile. However, still a similar pattern is visible.

3.7 Localization of flaws

In the previous section is shown that the rebound value obtained from an impact test clearly differs between a concrete tile and a rubber tile. For the rubber tile one can even see a pattern of the structure below the surface. The goal of this experiment is to see if the impact test can also be used to locate flaws in the concrete tile.

3.7.1 Design of experiment

In order to determine if the impact test can be used to locate structural flaws in the tile, a grid test will be done on a undamaged tile and a grid test will be done on a damage tile. This because the obtained rebound value is supposed to be a relative measurement. The rebound value is expected to be lower for a damaged tile than for an undamaged tile.

First will be investigated if the method can be used to locate a crack. A crack is induced into one tile, as shown in section 3.1.6. Accordingly a grid of impact tests over an area of 20 cm by 20 cm are done. This is also done for the undamaged tile. Then the rebound values will be compared, as it is a relative measurement, the rebound values for the undamaged tile will be subtracted from the rebound values of the cracked tile. This grid will be shown in the results, where a negative number will mean that the rebound value for the cracked tile is lower than the rebound value measured on the undamaged tile.

After the experiment to detect a crack, there will be investigated if the method can be used to detect a void in the concrete. A void is induced into a concrete tile, which is shown in section 3.1.6. Keep in mind that the rebound values for these tests will probably be different than earlier tests, as these concrete tiles are thicker than the tiles used for earlier tests. Same for the test on the cracked tile, a grid of impact tests will be done on the undamaged tile and on the tile with a void. As the detection of a void will also be a relative measurement, again a grid of differences in rebound value will be shown. A negative number means a lower rebound value for the tile with a void. This test will be repeated, but the tile with a void will be rotated -90° around its z-axis. It is expected that the tests on the damaged tile will yield lower rebound values. As discussed in the analysis, the tile with a void has a lower compressive strength. A lower compressive strength will cause to measure a lower rebound value.

In order to determine if this test is consistent, the impact test will be done ten times on the middle of the undamaged tile and be done ten times on the tile with a void. This in order to show the deviation of the test and if the difference caused by the void is within the deviation limits or not.

3.7.2 Results

In this section the results are shown of the experiments that are done in order to determine if the impact test is able to locate structural flaws in concrete.

In figure 3.53 the difference grid between an undamaged tile and a tile with a crack is shown, where the position of the crack is indicated with a line. The difference grid compares the tile with the crack, relative to the undamaged tile.

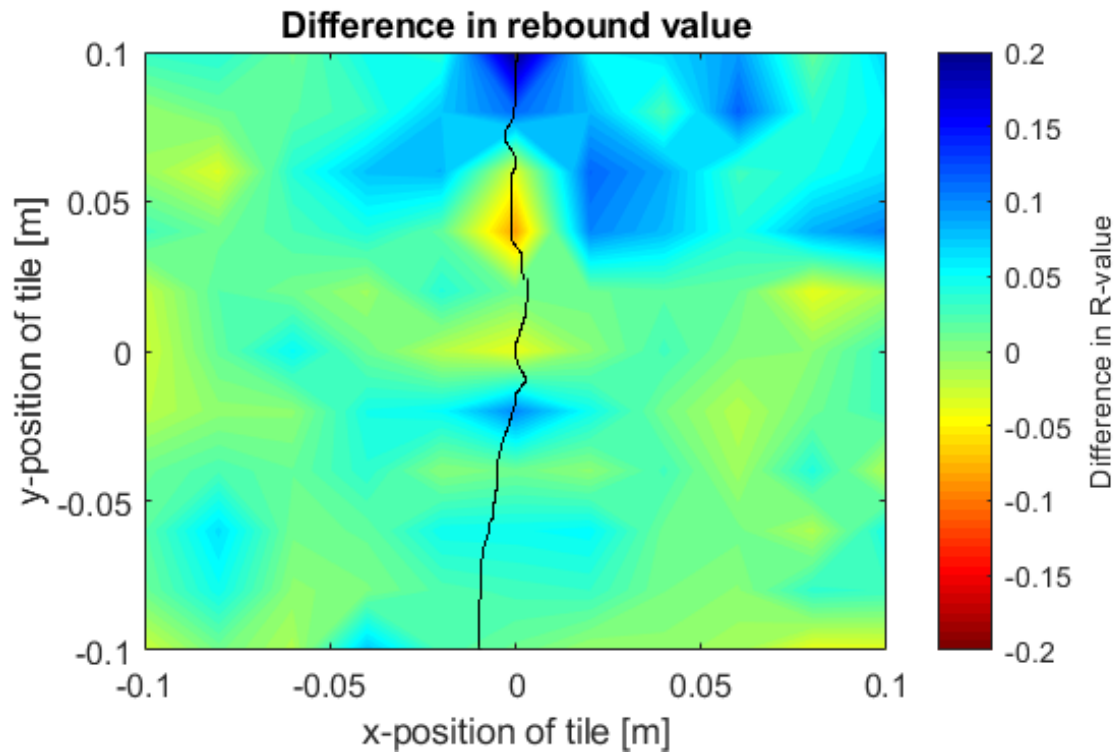


Figure 3.53: Measured difference in rebound values, detection of crack

In the previous figure, the blue in the top right corner probably originated from tape which was placed in the area of testing. In order to eliminate the influence of this tape, the test was done for a second time, but this time with the tape removed. The difference grid of the new test is shown in figure 3.54, where again, the crack is indicated with a line.

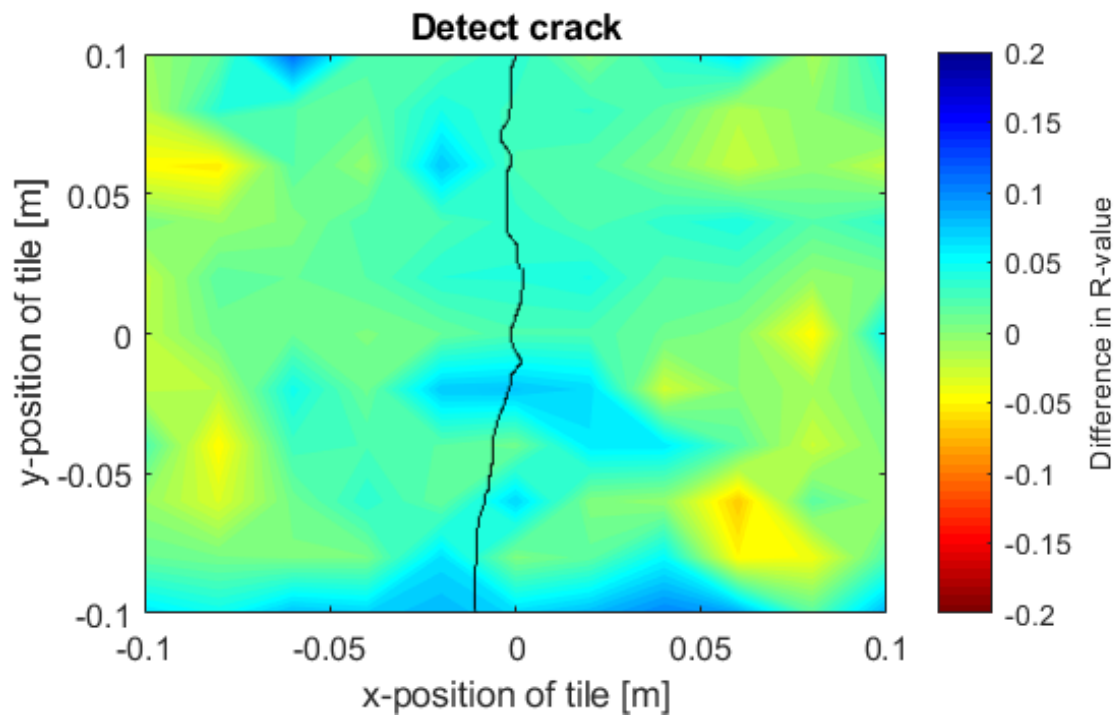


Figure 3.54: Detection of crack, second time

Figure 3.55 shows the difference in rebound values between a undamaged tile and a tile with a void, where the contour of the void is indicated with a line. A negative value indicates that the rebound value of the damaged tile is lower than the rebound value of the undamaged tile.

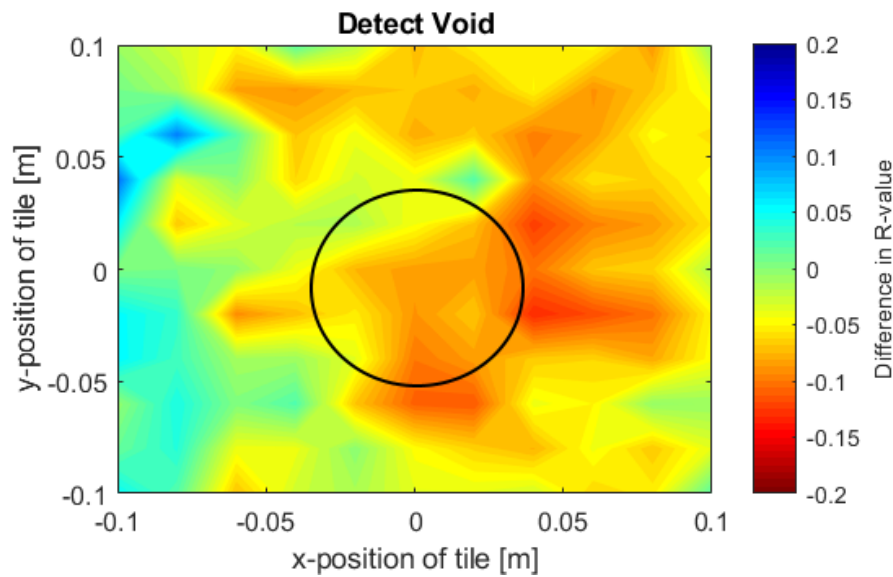


Figure 3.55: Measured difference in rebound values, detection of void

As mentioned, this test is repeated while the tile with the void is rotated -90° around its z-axis, which means that the top right corner of the tile in figure 3.55 is the bottom right corner of the tile for the graph in figure 3.56.

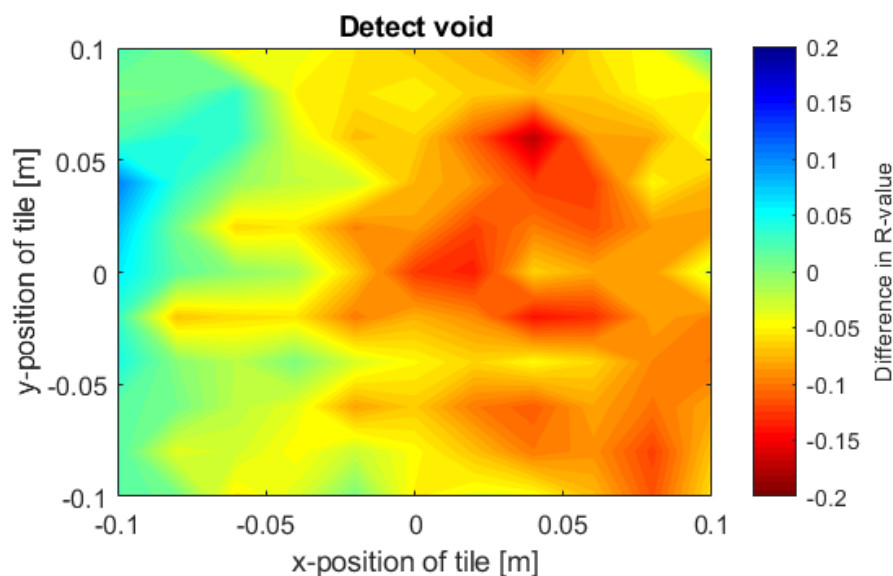


Figure 3.56: Detection of void, rotated the tile

In order to show the deviation of the test, the test is done ten times on the middle of the tile. The mean and the deviation of the impact test on an undamaged tile and a tile with a void are shown in figure 3.57.

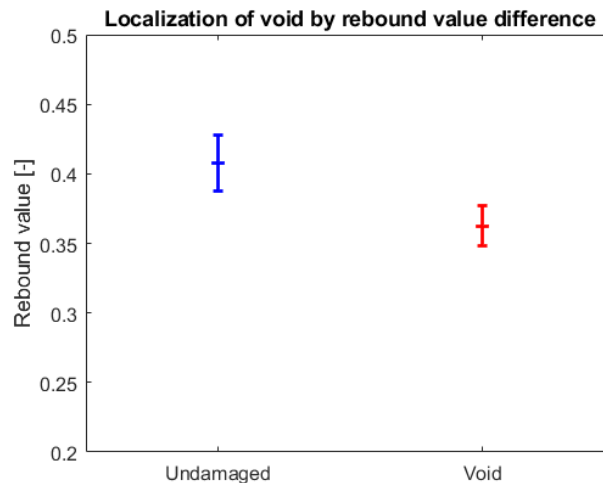


Figure 3.57: Deviation in detection of void

3.7.3 Discussion

Comparing the graph of figure 3.54 with the figure 3.53, it can be seen that redoing the test to eliminate the effect of the tape was necessary, as a clear difference can be seen between the two graphs. The behavior around the crack is however quite similar. Small deviations can be seen. Based on section 2.2.3 was expected that around the crack lower rebound values would occur. However, this is clearly not the case. As mentioned in section 2.2.3, the relation between cracks and the compressive strength has a diffuse character, in these experimental tests, the relation seems however to be non-existent. A small increase in rebound value can be noticed just below the middle of the tile, this is however not a result which could be used to identify the whole crack. The grids do however appear to show a bigger difference than the two tests on a single tile shown in figure 3.43. The values are however very close to the range of the deviation, so it does not seem that the method can be used to locate cracks.

Figure 3.55 does show a clear difference between an undamaged tile and a tile with a void. The difference is quite bigger than was shown in figure 3.43, and can be assumed to be larger than the deviation of the method. This results gives the indication that the method can be used to locate the void. Figure 3.56 again shows a large difference. The rotation of the tile is however not really visible between the two grids. The graph in figure 3.57 does show that the measured difference between the undamaged tile and the damaged tile is larger than the deviation of both tests, which makes clear that the void causes a measurable difference. This experiments show that the void can be identified. Additional research is however required in order to be able to localize a void.

3.8 Discussion of experimental study

In the previous chapter all sub-questions were answered theoretically. The last sub-question was answered theoretically. How can the rebound principle be used to locate structural flaws with a robotic arm? The answer on the last sub-question needed an experimental study, in order to determine if the proposed method is able to locate these flaws. The proposed method is the use of a virtual spring, attached to the end-effector of the robotic arm in order to induce an impact on the surface of the sample. Based on the relation between the rebound velocity and the impact velocity the rebound value can be determined. This rebound value is a relative measurement, which could be used to locate flaws. In this section this method is validated. The validation of the impact test showed that the method could still be used to obtain a certain rebound value. This measured rebound value showed quite some variation. Also for measuring the value for different positions showed quite some difference. A clear relation between the configuration of the arm and the measured rebound values could however not be found.

Different variables for the virtual spring were configured and tested, the results showed that from a certain impact energy, a higher impact energy results in a lower rebound value, which is in line with the theory based on the two types of Schmidt hammers. Subsequently the impact test has been used to determine the influence of a different elastic modulus of the sample. As expected from the theory, a lower elastic modulus increases the rebound value. Then the impact test was used in order to determine if the method could locate structural flaws. The test has been done on a tile with a crack and on a tile with a void. Both have been compared with an undamaged tile. The results showed a clear difference in rebound values between an undamaged tile and a tile with a void. Almost no difference has been measured between a tile with a crack and an undamaged tile. Repetition of these tests resulted in the same conclusion. In order to answer the following question: 'How can the rebound principle be used to locate structural flaws with a robotic arm?'

The results also showed that it is not to be expected that the method will be able to locate cracks in sewer pipes with this method. However, voids in concrete can be identified with a robotic arm by impacting with the surface with a certain impact energy, induced with a virtual spring, and use the relation between the rebound velocity and the impact velocity of the end-effector, the rebound value. This is a relative measurement, where the rebound value is lower for damaged concrete than for undamaged concrete. Both samples have to be in similar conditions. In the case of a concrete sewer pipe this can potentially be used by measuring the rebound value at several positions. Parts of the pipe with a void will be measured by obtaining a lower rebound value than parts that are not damaged. There has to be noticed that for the setup no sewer pipes were use, additional research is required in order to show that the method is actually able to locate the flaws from inside of the sewer pipe.

4 Conclusion and recommendations

In this section an answer will be given on the question: 'To what extent can interaction between a robotic arm and the surface of a concrete pipe be used to locate structural flaws of the pipe?' Also this research will be analyzed and recommendations for future research will be given.

4.1 Conclusion

The research question, 'To what extent can interaction between a robotic arm and the surface of a concrete pipe be used to locate structural flaws of the pipe?', is to be answered. This will be done in this section by answering the sub-questions separately.

4.1.1 Structural flaws

Which structural flaws in sewer pipes need to be located by physical interaction? In section 2.1 the structural flaws that occur in sewer pipes are mentioned and each flaw is discussed separately. Voids and cracks are considered to be the most important flaws that need to be localized by physical interaction inspection, because these flaws are not always visible on camera during in-pipe inspection. Moreover, voids can be very hazardous and cause tremendous damage to infrastructure and even cause injuries to citizens.

4.1.2 Relation between measurable physical properties and structural flaws

How do physical properties relate to the structural flaws of the pipe? In section 2.2 the relation between the measurable physical properties and structural flaws are discussed. It is mentioned that cracks and voids decrease the compressive strength of the concrete. The relation between the compressive strength and cracks is mentioned to be diffuse. The compressive strength of concrete seems to drastically reduce by voids in concrete. This relation does however not only depend on the size of the void, but also on the orientation of the void. No research has been conducted on the influence of a void behind the concrete, which could really be of added value to investigate as it is mentioned in section 2.1 to be a flaw which is important to be located if present.

4.1.3 Rebound hammers

What principle do the Schmidt hammer and Leeb hammer use to assess the concrete? The two rebound hammers apply an impact on the surface of the sample that needs to be assessed. The ratio between the rebound energy and the impact energy is used to determine the strength of the material and further referred to as the rebound value. This rebound principle depends on the lost energy due to plastic deformation. This rebound value actually measures a certain rate between the elastic modulus and the compressive strength. A lower elastic modulus will increase the ratio. A higher strength will also increase the ratio. This method is a relative measurement technique because the rebound value does depend on quite some variables. Due to a lot of research done in this field, a relation has been determined for concrete to relate the value to the compressive strength of the tested concrete.

4.1.4 Physical interaction with a robotic arm

How can the rebound principle be used to locate structural flaws with a robotic arm? The rebound principle can be mimicked by a robotic arm, in order to obtain a rebound value for a certain sample. This has been shown in the experimental study, chapter 3. By implementing a virtual spring attached between the sample and the end-effector of the robotic arm, via impedance control, the robotic arm applies an impact on the surface of the sample. The rebound value can be determined by dividing the rebound velocity with the impact velocity. The

method has been configured and validated. Subsequently has been tested on a rubber tile and a concrete tile. The results showed that a lower elastic modulus indeed yields a higher rebound value, while the compressive strength is lower. Finally the method has been tested on concrete with flaws, in order to determine if the method can be used to locate flaws. The results showed that the method could not be used to locate a crack. However, the results also showed that the method is able to identify a void in concrete, because the tile with a void results in a lower rebound value. Additional field research is required in order to prove that the method can indeed locate a void in sewer pipes.

4.1.5 Research question

To what extent can interaction between a robotic arm and the surface of a concrete pipe be used to locate structural flaws of the pipe? In this research is showed that a robotic arm is able to locate a void in a concrete tile. The proposed method in section 2.5 was not able to locate a crack in a concrete tile. It has however been shown that a robotic arm is able to locate a void in a tile by applying an impact test. For concrete with a void the rebound value measured will be significantly lower. The tests showed no difference between a concrete tile with or without a crack. In order to use an impedance controller to test the concrete, a torque controlled robotic arm which also measures its angular position in the joints is required.

4.2 Discussion

In this research the feasibility of locating structural flaws in concrete pipes by means of physical interaction with a robotic arm has been researched. A method has been proposed which has proven to be able to locate a void in concrete. A crack could not be located. Other flaws have not been researched as these flaws are clearly visible for CCTV which is currently used as inspection method. Interesting result of this research is that the rebound value can also be used to determine the elastic modulus of a material, instead of the strength of the material. Furthermore, the method showed to be able to determine the strength a material.

4.2.1 Advantages of proposed solution

In this section some advantages of the method will be discussed. First of all, a big advantage of this method is that a variation in impact energy can be achieved, which is different for the commonly used Schmidt hammers. This can not only be used for inspection goals, but also for research on the relation between the impact energy and the rebound value. Furthermore, the method can also be used for other implementations where robotic arms are used. For example for inspection of bridges or buildings. It can however also be used for inspection of other materials, like steel or rubber. Furthermore, the study showed that it is possible to identify a void behind the surface, without any visible damage on the surface. Therefore this method could be an a

4.2.2 Disadvantages of proposed solution

In this section some disadvantages of the proposed solution are discussed. A large disadvantage is that for this inspection, a robotic arm needs to be placed on a cart which will go into the sewer pipe. This will be an expensive way of trying to locate voids. Another con for the current implementation is that the impact is only done onto one direction. This is however easily resolvable by changing the configuration and applying a rotation on the stiffness matrix. Another big con is that the method appeared to be unable to locate cracks in sewer pipes.

4.3 Recommendations

For future research it is recommended to investigate if the rebound value can be determined without the addition of a virtual spring but by analyzing any impact. For this a clear relation

between the impact energy and the rebound value is required, as any impact can have any impact energy which is shown to influence the rebound energy. For implementing the proposed method, it is advised to implement it such, that it can inspect independent from the rotation, which will in theory not influence the rebound value. Research is however required in order to determine if this is the case in reality. Interesting for future research is to determine if the rebound value can be determined without the placement of a virtual spring, but by evaluating any impact. This could be useful for any robotic setup which has an unexpected collision, but can use this collision to gain knowledge about the structure it collided with. For inspection of sewer pipes it is advised to compare the performance of this method with the performance of measurement device with one degree of freedom. In case such a device has significantly less deviation, it could be better to chose such a device for inspection. In case a robotic arm is preferred for inspection, the method should be validated by testing from inside actual sewer pipes and determine if it can locate flaws. For this a robotic arm has to be used which can fit into such a pipe. For such research it is also advised to determine the influence of humidity and other flaws, like corrosion, on the rebound value. For future research it is also recommended to investigate the influence of a void behind the concrete on the measured rebound value. Since it was not part of this research, but locating a void behind the concrete could be considered an added value to the assessment method. Furthermore, in section 3.3 is mentioned that the robotic arm did also show movement in another direction than the impact direction. It is advised to use an impact device or impact strategy, where the rebound direction is constrained and perpendicular to the surface.

A Appendix Franka Emika Panda arm

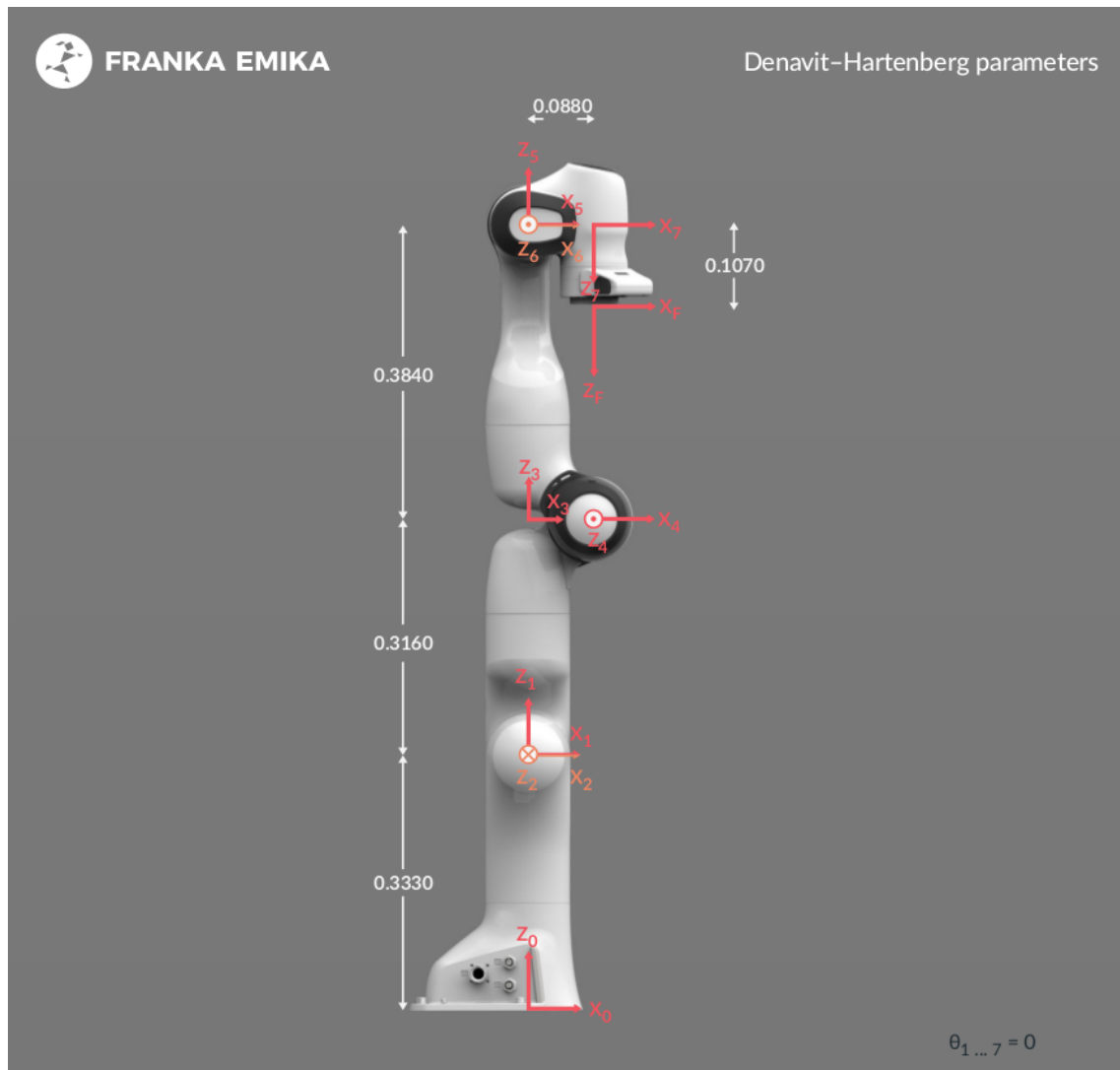


Figure A.1: dh-diagram of Panda arm

Name	Translation	Rotation	Elbow
\dot{p}_{max}	1.7 m s^{-1}	2.5 rad s^{-1}	$2.1750 \text{ rad s}^{-1}$
\ddot{p}_{max}	13 m s^{-2}	25 rad s^{-2}	10 rad s^{-2}
\dddot{p}_{max}	6500 m s^{-3}	12500 rad s^{-3}	5000 rad s^{-3}

Table A.1: Cartesian constraints

Name	Joint 1	Joint 2	Joint 3	Joint 4	Joint 5	Joint 6	Joint 7	Unit
q_{max}	2.8973	1.7628	2.8973	-0.0698	2.8973	3.7525	2.8973	rad
q_{min}	-2.8973	-1.7628	-2.8973	-3.0718	-2.8973	-0.0175	-2.8973	rad
\dot{q}_{max}	2.1750	2.1750	2.1750	2.1750	2.6100	2.6100	2.6100	rad s^{-1}
\ddot{q}_{max}	15	7.5	10	12.5	15	20	20	rad s^{-2}
\dddot{q}_{max}	7500	3750	5000	6250	7500	10000	10000	rad s^{-3}
τ_{jmax}	87	87	87	87	12	12	12	Nm
$\dot{\tau}_{jmax}$	1000	1000	1000	1000	1000	1000	1000	Nm s^{-1}

Table A.2: Constraints of each joint

Bibliography

- Al-Mosawi, A. (2015), Compression Strength of Composites and Rubber.
- Aslan, Z., R. Karakuzu and B. Okutan (2003), The response of laminated composite plates under low-velocity impact loading, **vol. 59**, no.1, pp. 119–127.
- Badarloo, B., A. Kari and F. Jafari (2018), Experimental And Numerical Study To Determine The Relationship Between Tensile Strength And Compressive Strength Of Concrete, *Civil Engineering Journal*, **vol. 4**, p. 2787, doi:10.28991/cej-03091198.
- Carlson, N. R. and S. A. Urquhart (2006), A sewer sinkhole study using TEM, **vol. 25**, no.3, pp. 348–350.
- Challis, J. H. (1999), A procedure for the automatic determination of filter cutoff frequency for the processing of biomechanical data, **vol. 15**, no.3, pp. 303–317.
- Counto, U. J. (1964), The effect of the elastic modulus of the aggregate on the elastic modulus, creep and creep recovery of concrete, **vol. 16**, no.48, pp. 129–138.
- Duran, O., K. Althoefer and L. D. Seneviratne (2002), Automated sewer pipe inspection through image processing, pp. 2551 – 2556, ISBN 0-7803-7272-7, doi:10.1109/ROBOT.2002.1013615.
- Dyskin, A., E. Sahouryeh, R. Jewell, H. Joer and K. Ustinov (2003), Influence of shape and locations of initial 3-D cracks on their growth in uniaxial compression, **vol. 70**, no.15, pp. 2115 – 2136, ISSN 0013-7944, doi:https://doi.org/10.1016/S0013-7944(02)00240-0.
<http://www.sciencedirect.com/science/article/pii/S0013794402002400>
- EngineersDaily (2019), ReboundHammerTest,
<http://www.engineersdaily.com/2011/04/rebound-hammer-test.html>,
 accessed: 2019-02-09.
- Ezeokonwo, J. (2000), Influence of Orientation and Size of Voids on Concrete Cube Strength, **vol. 19**, no.1, pp. 29–39.
- Fediuc, D. O., M. Budescu, V. Fediuc and V.-M. Venghiac (2013), Compression modulus of elastomers, **vol. 59**, no.2, p. 157.
- Hirsch, T. J. (1962), Modulus of elasticity of concrete affected by elastic moduli of cement paste matrix and aggregate, in *Journal Proceedings*, volume 59, pp. 427–452.
- Kaempfer, W. and M. Berndt (1999), Estimation of service life of concrete pipes in sewer networks, *Durability of Building Materials and Components*, **vol. 8**, pp. 36–45.
- Karoui, T., S.-Y. Jeong, Y.-H. Jeong and D.-S. Kim (2018), Experimental Study of Ground Subsidence Mechanism Caused by Sewer Pipe Cracks, *Applied Sciences*, **vol. 8**, p. 679, doi:10.3390/app8050679.
- Kompatscher, M. (2004), Equotip-rebound hardness testing after D. Leeb, in *Proceedings, Conference on Hardness Measurements Theory and Application in Laboratories and Industries*, volume 1, Citeseer, pp. 1–12.
- Kovler, K., F. Wang and B. Muravin (2018a), Testing of concrete by rebound method: Leeb versus Schmidt hammers, **vol. 51**, no.5, p. 138, ISSN 1871-6873, doi:10.1617/s11527-018-1265-1.
<https://doi.org/10.1617/s11527-018-1265-1>
- Kovler, K., F. Wang and B. Muravin (2018b), Testing of concrete by rebound method: Leeb versus Schmidt hammers, **vol. 51**, no.5, p. 138.
- Kvgd, B. and A. Yelisetty (2014), *CONDITION ASSESSMENT OF EXISTING STRUCTURES USING NDT TECHNIQUES*, Ph.D. thesis.

- Maruyama, I., H. Sasano, Y. Nishioka and G. Igarashi (2014), Strength and Young's modulus change in concrete due to long-term drying and heating up to 90 °C, *Cement and Concrete Research*, **vol. 66**, p. 48–63, doi:10.1016/j.cemconres.2014.07.016.
- NWO (2017), Technology Innovation for Sewer Condition, Assessment – Long-distance Information-system (TISCALI), accessed: 2018-10-09.
<https://www.nwo.nl/onderzoek-en-resultaten/onderzoeksprojecten/i/97/27097.html>
- Ott, C., A. Albu-Schaffer, A. Kugi, S. Stamigioli and G. Hirzinger (2004), A passivity based Cartesian impedance controller for flexible joint robots - part I: torque feedback and gravity compensation, in *IEEE International Conference on Robotics and Automation, 2004. Proceedings. ICRA '04. 2004*, volume 3, pp. 2659–2665 Vol.3, ISSN 1050-4729, doi:10.1109/ROBOT.2004.1307462.
- Patel, S. D., S. Ahmad and P. Mahajan (2014), Reliability Analysis of a Composite Plate under Low-Velocity Impact using the Gaussian Response Surface Method, **vol. 15**, no.3, pp. 218–226, doi:10.1080/15502287.2014.882439.
<https://doi.org/10.1080/15502287.2014.882439>
- Pigeon, P., P. DiZio and J. R. Lackner (2013), Immediate compensation for variations in self-generated Coriolis torques related to body dynamics and carried objects, *American Journal of Physiology-Heart and Circulatory Physiology*.
- RAM (2019), Tiscali,
<https://www.ram.ewi.utwente.nl/research/project/tiscali.html>,
accessed: 2019-05-09.
- Randrup, T. B., E. G. McPherson and L. R. Costello (2001), Tree root intrusion in sewer systems: review of extent and costs, **vol. 7**, no.1, pp. 26–31.
- ReboundGuide (1993), *The title of the work*, testcoate-USA,
https://www.testcoat-usa.com/media/wysiwyg/Concrete_Hammer_TC_120_USER_S_MANUAL.pdf, accessed: 2019-02-21.
- Smith, G. (1989), Padding point extrapolation techniques for the butterworth digital filter, **vol. 22**, no.8, pp. 967 – 971, ISSN 0021-9290, doi:https://doi.org/10.1016/0021-9290(89)90082-1.
<http://www.sciencedirect.com/science/article/pii/0021929089900821>
- StateOfIndiana (2014), Inspection Manual For Precast Concrete Pipe And Structures.
<https://www.in.gov/indot/files/InspectionManualForPrecastConcretePipeAndStructures.pdf>
- Stramigioli, S. and H. Bruyninckx (2001), Geometry and screw theory for robotics.
- Szilágyi, K., A. Borosnyói and I. Zsigovics (2015), Understanding the rebound surface hardness of concrete, **vol. 21**, no.2, pp. 185–192.
- Tacoma (2019), accessed: 2019-02-21.
<https://cms.cityoftacoma.org/wastewater/sewerinspection/repair.pdf>
- Tort, C., A. M Asce, J. Hajjar and F. Asce (2010), Mixed Finite-Element Modeling of Rectangular Concrete-Filled Steel Tube Members and Frames under Static and Dynamic Loads, *Journal of Structural Engineering-asce - J STRUCT ENG-ASCE*, **vol. 136**, doi:10.1061/(ASCE)ST.1943-541X.0000158.
- Vecchio, F. J. and M. P. Collins (1993), Compression response of cracked reinforced concrete, **vol. 119**, no.12, pp. 3590–3610.
- Vonk, R. A. (1992), Softening of concrete loaded in compression.
- Warren, C. (1953), Determination of Properties of Air Voids in Concrete, , no.70.

- Winkler, S. and J. A. Matthews (2014), Comparison of electronic and mechanical Schmidt hammers in the context of exposure-age dating: are Q-and R-values interconvertible?, **vol. 39**, no.8, pp. 1128–1136.
- Winter, D. A. (2009), *Biomechanics and motor control of human movement*, John Wiley & Sons.
- YILMAZ, N. G. and R. M. GÖKTAN (2018), Analysis of the Leeb Hardness Test Data Obtained by Using Two Different Rock Core Holders, **vol. 22**, no.1, pp. 24–31.